*Heat Transfer Research* 44(3–4), 347–390 (2013)

# THERMAL ANALYSIS AND EXPERIMENTS OF LASER–TISSUE INTERACTIONS: A REVIEW

*Amir Yousef Sajjadi,*[1,*] *Kunal Mitra,*[1] *& Zhixiong Guo*[2]

[1]*Department of Mechanical and Aerospace Engineering, Florida Institute of Technology, Melbourne, FL 32901, USA*

[2]*Department of Mechanical and Aerospace Engineering, Rutgers, The State University of New Jersey, Piscataway, NJ 08854, USA*

[*]Address all correspondence to Amir Yousef Sajjadi E-mail: asajjadi@my.fit.edu; asajjadi@nmr.mgh.harvard.edu

*Studying the interaction of ultrashort pulse lasers with biological tissues and the corresponding mathematical modeling of possible thermal damage is of fundamental importance to the understanding of laser–tissue interaction for advancing surgical application of lasers. The objective of this paper is to review the existing techniques for thermal analysis of laser–tissue interaction, focusing on temperature rise and plasma-mediated ablation. Different laser–tissue interaction mechanisms are discussed, and the existing techniques for characterization of extent of damage are presented. A novel approach of using a focused laser beam from an ultrashort pulse laser source to ablate the subcutaneous tumors with minimal thermal effects is introduced. The extent of laser-induced damage is studied by determining the space–time expression patterns of heat shock proteins.*

**KEY WORDS:** *thermal ablation, heat shock proteins, tumor removal, short-pulse laser, laser–tissue interaction, plasma mediated ablation, HSP70, HSP47, ablation modeling*

## 1. INTRODUCTION

Lasers offer potential applications in tumor ablation and therapies (Sajjadi et al., 2009, 2011a,c, 2012). Techniques including laser-induced hyperthermia (Waldo et al., 1998; Panjehpour et al., 1991; Robinson et al., 1998), laser interstitial thermal therapy (LITT) (Pech et al., 2004), and laser immunotherapy (O'Neal et al., 2004) have been developed for successful ablation of subsurface tumors. All these techniques utilize a photothermal mechanism for tumor ablation by delivering thermal energy at the tumor site. In laser-induced hyperthermia and LITT, the laser heats both normal and tumor tissue indiscriminately, which often results in damage and death of the surrounding healthy tissues. On the contrary, laser immuno-

1064-2285/13/$35.00  

therapy utilizes selective absorption of light energy in the tumor tissue by injecting photoabsorptive dyes at the tumor location. Even so, laser immunotherapy (as well as LITT and laser-induced hyperthermia) traditionally utilizes continuous-wave (CW) or long-pulse laser sources often producing heat-affected zones, which are larger than the boundaries of the tumor. This in turn leads to collateral damage of healthy tissue.

Recently, ultrashort pulse lasers (USP lasers), having pulse widths ranging from picoseconds down to femtoseconds, have been used in a wide spectrum of emerging biomedical technologies including laser surgery (Anderson and Parrish, 1983; Niemz, 1996; Bass and Treat, 1995; Anderson, 2003; Han et al., 2004; Koeing et al., 2005; Niemz, 2003; Pal et al., 2009; Sajjadi et al., 2011c; Sajjadi et al., 2013; Sajjadi et al., 2012; Fahey et al., 2008) and the manipulation of biological architecture and biochemistry on a microscopic scale (Vogel et al., 2005). Precise control over the laser energy delivery is the rationale for favoring short-pulse lasers over continuous lasers. Short-pulse lasers induce a thermal incision with a time course that is shorter than the thermal relaxation time of the material and therefore minimize the thermal damage zone.

Tissue removal by using lasers, which produce minimal damage to the adjacent structures, is the surgical goals for a number of high precision medical procedures such as ophthalmology, dentistry, thermal therapy, and angioplasty. Among the various therapeutic applications of lasers, minimally invasive technique of irradiating tumor has received significant attention from researchers (Mito, 1996). Laser interaction with tissue can be categorized into several mechanisms, which include photothermal, photomechanical (or photoacoustical), photochemical (Verena et al., 2004), photoablation (Vogel and Venugopalan, 2003), and plasma-mediated ablation (Niemz et al., 1991). The focus of this paper is to develop a minimally invasive technique of tumor irradiation using the photothermal mechanism.

It has been well established that the tissues are sensitive to the temperature rise. The thermal impact on tissue changes drastically when the temperature rise exceeds $43^{o}$C (Jeong et al., 2003). For example, in laser hyperthermia, the temperature of a pathological tissue is often elevated to be from $42^{o}$C to $45^{o}$C such that the growth of malignant tumor can be retarded. In laser coagulation, laser beams can cause immediate irreversible damage of pathological cells by heating them up to above $60^{o}$C. In laser surgery, a laser beam can vaporize and cut tissues like a scalpel when tissue temperature is heated to as high as $100^{o}$C. No matter which medical treatment is performed, a thorough understanding of the damage distribution within both pathological tissue and the surrounding healthy tissue is imperative (Zhou et al., 2007).

It has been demonstrated that a peak temperature above $60^{o}$C is required to ensure complete tumor necrosis without any post-treatment trauma. However, it has been also observed that temperature required to kill the tumor tissue depends on the exposure time. Robinson et al. (1998) have predicted that temperature eleva-

tion to at least 56°C in 1 s or more should be sufficient for kiling cancer cells. Thus, there is no general consensus in the literature about the exact extent of temperature rise and irradiation time necessary for complete tumor ablation.

In spite of the availability of many temperature-monitoring techniques, it is not possible to measure temperature at each and every location of the tissue. Therefore, it is required to develop a flexible numerical model that can predict temperature of any desired location in the tissue medium. Furthermore, development of such kind of model helps in designing new techniques that can ensure accurate and controlled deposition of energy into the exact location in biological tissues with minimum collateral thermal damage to the adjoining healthy tissue. Substantial efforts have been made previously to develop a complete theoretical model based on Pennes' bio-heat transfer equation considering the inherent complexity of the heat transfer process in tissue medium (Pennes, 1984). Such previous works have focused on two main categories: one in which there is internal source of heat generation such as metabolism (Welch, 1984) and the other in which an external source of heat generation such as laser irradiation is considered (Prahl et al., 1997). It has already been demonstrated that Penne's bio-heat transfer model, which accounts for laser penetration and subsequent absorption of laser energy within the tissue, is a good approximation for predicting tissue temperature profiles for the case of laser irradiation of tissues (Diaz et al., 2001; Sajjadi et al., 2008c).

McKenzie (1990) discussed a broad range of applications of the thermal response of soft tissue to laser radiation and clearly explained the basic principles of thermal laser–tissue interaction. The basic principles that govern the relationship between thermal exposure (temperature and time exposure) and thermal damage, with emphasis on normal tissue effects has been reported in the literature (Dewhirst et al., 2003). Several published computer models have predicted heat generation, transient temperatures, and thermal damage in tissues, but few works have compared modeling results with the experimentally measured temperature. Aksan et al. (2005) presented the modeling of temperature and thermal damage zone for collagenous tissue heated with monopolar and bipolar lasers and validated the results with experimentally measured data. Temperature distribution and damage as a function of power, exposure duration, and spot size for optical properties associated with 2000-nm irradiation of pig skin have been obtained numerically using finite-element model and validated experimentally by Chen et al. (2006). Welch (1975) developed a model that simulates light propagation, heat generation, transient temperature response, and thermal damage produced by a radically symmetric laser beam of normal incidence.

Measurement of temperature rise in tissues during laser irradiation helps determine the size of the heat-affected zone, but it does not show the extent of cellular damage produced during laser irradiation. A detailed histological study is therefore required to correlate energy input, temperature rise, and the extent of cellular damage necessary to evaluate the ablated tissue volume. The ability to provide direct

visual information of thermal damage and ablated zone produced by the laser made this technique essential for both fundamental and application oriented studies. Histological analysis of morphological changes has been used extensively to study the mechanism of tissue ablation (Boppart et al., 1999; Youn et al., 2006).

### 1.1 Interaction of Laser with Biological Tissue for Therapy

Among the many clinical applications of medical lasers, a unique capability of short-pulse lasers is that they allow selective and precise removal of tissue with minimal damage to the surrounding tissue mass (Niemz, 1996). This property is important in high-precision medical procedures such as ophthalmology, dentistry, angioplasty, and thermal therapies. The nature of tissue damage due to laser irradiation varies based on the laser wavelength, pulse duration, beam characteristics, and tissue properties (Niemz, 1996; Vogel et al., 1998; Welsh and Van Gemert, 1995; Sajjadi et al., 2008a). There are a few mechanisms of laser–tissue interaction that can occur individually or in combination depending upon the laser parameters. The photothermal effects are most commonly observed and can be quantified by measuring the temperature rise at the point of irradiation. In a photochemical reaction, the release of free radicals due to the laser energy causes damage to the tissue (Jaques, 1991). Photomechanical tissue destruction involves the generation of shock waves that propagate through tissue and can cause ablation at the surface of the tissue (Chen et al., 1996). Each mechanism can contribute to ablation in different manners. In most of these mechanisms, the temperature rise causes thermal damage to the adjacent tissue. An excellent overview of these three physical mechanisms of interaction was presented by Jacques (1992).

Niemz (2003) added another three mechanisms into the category of interactions. Photoablation occurs when ultraviolet (UV) photons are absorbed. Since high-energy UV photons are more energetic than most chemical bonds that hold molecules together, the dissociation of the molecules is caused. This phenomenon is followed by a rapid expansion of the irradiated volume and ejection of the tissue debris from the surface. In a plasma-mediated ablation, a free electron is accelerated by the intense electric field in the vicinity of laser beam focus. By colliding with a molecule and freeing another electron, it initiates a chain reaction of similar collisions, which is called 'avalanche ionization', resulting in plasma: a soup of ions and free electrons. Plasma-mediated ablation can remove the tissue in a nonthermal manner. This can be achieved when a tightly focused laser with pulses on the order of picoseconds or femtoseconds is used (Fischer et al., 1994; Niemz, 1996) and the irradiation is over a threshold of optical-breakdown. In nonthermal or cold evaporation of tissue, nontargeted tissue remains free of thermal or mechanical damage (Sajjadi, et al., 2012). Photodisruption is an extreme of mechanical effect that may occur during plasma-mediated ablation with extremely strong laser intensity, leading to bubble formation and shock wave generation. If breakdown occurs inside a soft tissue or fluid, additional cavitation and jet formation may take place.

Each mechanism is described briefly below. Many investigators have studied impacts of different laser ablation mechanisms and their characteristics in detail.

### 1.1.1 Photothermal ablation

Photothermal laser–tissue interaction occurs when the laser energy is absorbed by the target tissue and converted into heat. The effect on the tissue depends on the amount and rate of deposited heat. A low-temperature elevation over a long time (less than $10^{o}$C over many seconds or minutes) usually causes cell damage or death without causing structural alternation to the tissue (photoheating). Greater temperature elevation at shorter time intervals (20–$30^{o}$C in approximately 1 s) causes photocoagulation of the tissue with irreversible structural damage to the tissue due to the denaturation of tissue proteins and cellular death. The deposition of laser energy in shorter intervals (much less than 1 s) heats the tissue above its boiling point and may cause thermally mediated tissue removal by explosive vaporization (photovaporization). The wavelength of the laser, laser power (intensity), laser pulse width, duration of laser irradiation, and optical properties of the tissue determine which of these photothermal effects predominate (Waynant, 2002).

Hyperthermia treatment of tumors is based upon a selective tumor response during tissue heating (Hahn, 1979). Research has shown that high temperatures of at least $41^{o}$C can damage and kill cancer cells (Robinson et al., 1998). It is anticipated that hyperthermia treatment kills cancer cells by damaging proteins and structures within the cells, thus shrinking the tumors. Primary malignant tumors have poor blood circulation, which makes them more sensitive to changes in temperature. The thermal impact on tissue changes drastically when the elevation of temperatures exceed $43^{o}$C leading to tumor irradiation (Dewhirst et al., 2003; Arora et al., 2005). Disruption of tissue starts at temperatures above $60^{o}$C due to protein denaturation between $60^{o}$C and $65^{o}$C and then by collagen denaturation at $80^{o}$C. Some other applications are in laser vascular treatment (Ozturk et al., 2004, Raskin and Fany., 2004; Sajjadi et al., 2008b) and laser tissue welding and soldering (Xie et al., 2001). Above $80^{o}$C, tissue vaporization takes place, ultimately leading to carbonization (Steiner, 2003).

### 1.1.2 Photomechanical ablation

High-intensity pulse lasers can produce shock waves when incident on tissue and these shock waves can disrupt tissue. When heat is deposited in the tissue and the main mechanism is photothermal, thermoplastic expansion of the tissue can result in photomechanical ablation of the tissue. Induced stress will propagate as a wave into the surrounding tissue. The optical properties of the tissue, laser wavelength, and pulse duration regulate the ablation mechanism. Popular applications of photomechanical ablation are used in the treatment of cataracts (Heisterkamp et al., 2003) and the treatment of kidney stones (Rink et al., 1995).

### 1.1.3 Photochemical ablation

Photochemical interactions occur at very low power intensities (1 W/cm$^2$) and long exposure time (seconds for continuous-wave lasers). Laser wavelength, intensity, and duration are the parameters that should be selected carefully to ensure the radiation distribution inside the tissue. In most cases, lasers in the visible range are used because of their high optical penetration depths and efficiency. The photochemical effect occurs due to the breaking of chemical bonds in the molecules by laser radiation. Photosensitizers such as hematoporphyrin derivatives, which accumulate inside the tumor, are being used for treatment of cancer with a technique called photodynamic therapy (Kimel et al., 2004). During photodynamic therapy (PDT), the photosensitizers absorb laser irradiation and trigger chemical reactions resulting in the formation of toxic biochemical species such as reactive oxygen species. The tissue destruction is caused by the cytotoxity of reactive oxygen species, especially singlet oxygen. Other applications of PDT include treatment of primary carcinoma, cutaneous lesions, and chronic stable plaque psoriasis (Gomer et al., 1989). The major use of photochemical ablation is in cancer therapy and treatment of tumorous tissues deep inside the body.

### 1.1.4 Plasma-mediated ablation

Plasma-mediated ablation (plasma-induced ablation) takes place when the energy densities exceed a threshold of $10^{11}$ W/cm$^2$ in solids and fluid, or $10^{14}$ W/cm$^2$ in air. A phenomenon called laser-induced optical breakdown (LIOB) occurs at these power densities that causes transformation of matter to plasma (Niemz, 2003) via avalanche ionization.

High-density laser energy causes the material to ionize when the energy threshold reaches the optical beakdown of the material. The plasma created by LIOB is a state of matter characterized by ions and free electrons. Once the plasma is formed, it will absorb subsequent pulses of laser energy and initiate a rapid vaporization of adjacent tissue. When plasma-mediated ablation occurs, non-targeted materials remain free of thermal or mechanical damage (Sajjadi et al., 2011a). Ultrashort pulse lasers can initiate this process because of their ability to deliver high laser intensity at lower energies. Lasers have been successfully used to produce desired ablation zones with precise crater depth in bones and skin (Kim et al., 2001, Youn et al., 2006). To shape the human cornea, a precision of a fraction of a micron is required (Kurtz et al., 1997). Guo's group used such a technique for processing and decontaminating donor tissues in recent years (Huang and Guo, 2009, 2010; Wang and Guo, 2010). In order to evaluate the degree of thermal damage, the histology of some ablated samples was analyzed. No visible thermal damage was found when a single well-controlled ablation occurs. When multiple ablation events are applied for in the same spot, however, thermal damage within a 10-micrometer zone was observed. Recently Jiao and Guo (2011) modeled plasma-formation processes during USP laser-induced ablation in water and tissue.

They further postulated that a critical seed free electron density exists in order to trigger avalanche ionization (Jiao and Guo, 2012).

## 1.2 Laser Delivery Methods

In most existing laser-induced percutaneous tumor ablation techniques such as hyperthermia and LITT, either collimated or diffused laser beams are used, resulting in much of the energy being absorbed by tissues at the skin surface and very little remaining energy penetrating the skin. Such drawbacks of collimated laser beams can be minimized if the beam from an ultrashort pulse laser source is focused directly at the targeted subsurface location. That is, focusing the laser beam at the desired treatment location depth can reduce the problem of absorption of laser energy at the skin surface.

### *1.2.1 Advantages of using a focused beam from an ultrashort pulse laser source*

While a focused beam of an ultrashort pulse laser may provide a significant advantage for biomedical applications over CW lasers and collimated beams, the parameters of its use must be carefully calibrated for optimal effect. That is, irradiation of the target material by repetitive pulses can lead to cumulative effects that can be tailored to attain complete targeted ablation with minimal collateral damage. When a tightly focused laser with pulses on the order of picoseconds or femtoseconds is used, a cold evaporation of the tissue occurs (Fischer et al., 1994; Niemz, 1996), but even ultrashort laser pulses (duration shorter than 10 ps), each of which has negligible thermal effect, may add up to produce a significant temperature rise at the focused spot (Welsh and Van Germet, 1995). If the time between the laser pulses is small relative to the time required for heat to diffuse out of the vicinity of the focal volume, heat can accumulate near the focal region. Despite the low total energies required, femtosecond laser ablation can thus lead to significant thermal and chemical effects under certain conditions, and the cumulative effects of repetitive pulses may occur at energies below the threshold for photodisruption. Better control of the exposure time (and thus control of potential thermal effects) can be achieved by translating the beam at specific velocities to irradiate the desired tissue volume. Thus, the selection of optimal scanning beam velocity is critical to control the size of ablation volume and to eliminate possible thermal damage in surrounding tissue.

The mechanisms of action of continuous and long-pulse laser ablation of tissue are very different from the mechanism of USP laser–tissue interaction, and these differences have important implications for the use of lasers in therapeutic applications. In conventional laser ablation techniques utilizing continuous or long-pulse lasers, linear absorption underlies the dominant mechanism of ablation, and heat is dissipated out of the laser-stimulated area by thermal diffusion. Such thermal diffusion may cause significant collateral damage to the surrounding healthy tissue. On the other hand, damage produced by ultrashort pulse laser treatment is more confined because the pulse duration is less than the time required for energy dif-

fusion from the region of laser excitement. Ultrashort pulse (picosecond and femtosecond) laser ablation causes the formation of plasma, is a nonlinear phenomenon, and is independent of material properties (Welsh and Van Germet, 1995). Because plasma-mediated ablation is nonlinear, the ablation threshold is independent of tissue linear absorption for ultrashort pulses (Sajjadi et al., 2011a). Furthermore, because short pulses require less energy than longer pulses to reach the threshold intensity required for optical breakdown, short pulses deposit less energy in the material and this lower energy deposition provides more precise ablation (Chung and Mazur, 2009). Thus, pulse lasers having pulse durations of picoseconds or femtoseconds make ideal tools for heat-sensitive soft tissues such as the cornea and the dermis/epidermis (Loesel et al., 1996, 1998; Fischer et al., 1997; Neev et al., 1996; Manstein et al., 2004; Khan et al., 2005; Sajjadi et al., 2010), because ultrashort laser treatment provides high precision and minimal collateral tissue damage (Han et al., 2004; Koeing et al., 2005; Niemz, 2003; Bille et al., 2002; Armstrong et al., 2002; Vogel et al., 1998; Sajjadi et al., 2013).

### 1.3 Selection of the Optimum Wavelength for Subsurface Ablation

Infrared lasers have been used for biomedical applications involving human tissues. For example, 1700-nm femtosecond lasers have been used to produce subsurface incisions in human sclera (Sacks et al., 2001), and a 1552-nm femtosecond laser generated surface lesions in human dermis via plasma-mediated ablation without any alternation in tissue morphology (Huang and Guo, 2009). Nonablative fractional photothermolysis is currently approved by the US Food and Drug Administration (FDA) for the treatment of pigmented lesions, periorbital rhytides, skin resurfacing, melisma and soft tissue coagulation, acne and surgical scars, and actinic keratoses (Allemann and Kaufman, 2010). The 1550-nm wavelength is the ideal for fractional resurfacing, allowing sufficient penetration into the tissue (Thongsima et al., 2010; Helbig et al., 2010). At the wavelengths in which the skin has higher absorbance, e.g., at the 1440 nm, the beam penetrates superficially, providing less volume of tissue treated and ultimately reducing the amount of tissue affected by the collagen remodeling process. The ultrashort pulse laser of 1552-nm wavelength is a relatively new development, and was conceived as an optimal compromise between the effects of optical scatter and optical absorption in silica-based fiber optics for industrial applications. That is, at longer wavelengths optical absorption increases, and at shorter wavelengths optical scatter increases at fiber defects. A wavelength of 1550 nm represents the best compromise in that it produces the lowest absorption and the lowest scatter (Sajjadi et al., 2011a). In addition, lasers above 1400-nm wavelength (and particularly noncollimated beams) are relatively eye-safe because their output is not readily transmitted through the cornea. Finally, because the threshold for plasma optical breakdown, and therefore ablation threshold, decreases with increasing tissue absorbance for subnanosecond pulses (Oraevsky et al., 1996) and because biological tissues exhibit significant ab-

sorbance at this wavelength, 1552 nm may provide a novel mechanism for therapeutic ablation, particularly when delivered via fiber optics. Therefore, the goal of the work presented here was to determine the efficacy of a focused-beam 1552-nm ultrashort pulse laser for subcutaneous tumor ablation.

## 2. CHARACTERIZATION OF THERMAL EFFECTS DURING AND AFTER LASER TREATMENT

Numerous methods are used to study the extent of laser-induced effects. Some are noninvasive like measuring the temperature during and after laser-irradiation, and some are invasive and provide useful information regarding the structure and morphology of the tissue after laser-induced damage.

### 2.1 Instantaneous Thermal Effects

Monitoring the temperature rise during laser irradiation of tumors is required to obtain the specific temperature rise at the desired location with the least possible thermal damage of healthy tissues. Existing temperature measurement techniques can be classified into three different types: volumetric thermometry, surface thermometry, and local (point) thermometry. In volumetric thermometry, the temperature at different points within a significant volume is measured. The most popular example of this method is Magnetic Resonance Imaging (MRI) temperature imaging. High contrast and spatial resolution of three-dimensional images of a tumor and surrounding normal tissues has made MRI the most popular imaging technique (Mark et al., 2004). In surface thermometry, temperature on the surface is monitored by a thermal sensor like an infrared (IR) camera. Examples are in ablation of tissues (Dayan et al., 2004) or monitoring the skin temperature during laser therapy of port wine stains (Torres et al., 1999). In local thermometry, point temperature probes such as a thermocouple or a fiber optic sensor are inserted at the desired location and the local temperature is measured. Some of their advantages are their simplicity and low cost compared to MRI or an infrared camera (Sun et al., 1989, Wilkens et al., 1999; Davidson et al., 2005). However, thermocouple measurement is an indirect measurement and needs to be calibrated before use. Some applications of the thermocouple use are in temperature measurement during laser irradiation in porcine and human breast tissue (Robinson et al., 1998), and LITT of breast cancer (Manns et al., 1998; Milne et al., 2000).

### 2.2 Histological Analysis

A detailed histology is required to study the structural and morphological alternations during laser irradiation (Wells et al., 2005). The size and extent of thermal damage can be estimated using histology. Histological studies can be used to determine the ablation depth and extent of thermal necrosis of tissue during laser welding (Fried and Walsh, 1998), treatment of muscles (Gratzl et al., 1991), and laser-induced thermal injury of blood vessels (Dai et al., 2005). Histological meth-

ods are used to study morphological changes in laser immunotherapy treatments of metastatic mammary tumors (Nordquist et al., 1998), fractional photothermolysis (Manstein et al., 2004; Laubach et al., 2006), and nonablative dermal remodeling (Khan et al., 2005). Detailed histological study of rat skin tissue ablated with Er:YAG laser at low laser intensity and at various repetition rates was performed and the H&E (hemotoxylin and eosin) stained sections clearly demonstrate the depth of dermal collagen coagulation (Majaron et al., 2000).

Depending on the type of tissue, various sectioning techniques such as frozen sectioning technique or paraffin embedding technique are used in histological studies (Presnell and Schreibman, 1997). The frozen sectioning method is simple and eliminates lengthy tissue processing techniques required in other methods. Therefore, in this research, the frozen section technique was used for histological analysis. The depth and radial spread of ablation can be observed using a light microscope.

### 2.3 Immunohistochemistry

In order to develop the most useful laser-based clinical approaches, it is important to understand both the mechanisms of interaction between laser and tissue and the extent of tissue damage for given parameters of laser irradiation (wavelength, fluence, duration, etc.). It has been shown that the wound recovery period is proportional to the size of a laser-induced wound (Sherratt and Murray, 1992), but much more needs to be done to fully understand the extent of laser-induced damage instantaneously after irradiation and over the course of time following irradiation, and to understand the process of wound healing in order to enhance its rate. That is, studying the effects of laser treatment immediately following irradiation of living tissues provides vital information regarding the size, type, and extent of damage, but damage parameters may change as the lesion "matures". Therefore, in order to understand the true extent of damage and the healing process, analysis of the effects of laser–tissue interaction must be performed over time following irradiation.

Instantaneous laser-induced damage to the tissue can be investigated by measuring thermal effects of laser irradiation on tissue during the laser procedure. Based on the interaction mechanism, an energy threshold is necessary to make temporary or permanent changes in tissue structure. The temperature profile in the tissue around the laser-irradiated region gives insight into radial energy spread and therefore the extent of damage in tissue surrounding the ablation zone. Histological studies may provide valuable insight by displaying the size and extent of cellular damage and tissue alteration produced during laser–tissue interaction. In addition to standard histology, immunohistochemical localization and immunoblotting of proteins specific to the damage and healing processes can be utilized to show the extent of injury to the tissue and the process of healing. Heat shock proteins are a group of proteins whose expression patterns can give insights into the extent of damage and the healing process.

### 2.3.1 Heat shock proteins

Several mechanisms have been developed in all mammals to survive a changing environment as well as to cope with stress. Altering cellular structure and function to deal with adverse conditions or temporary alteration in gene expression to survive changing environments are among these mechanisms. Synthesis and function of heat shock proteins (HSP) are among the important mechanisms prompted by stress. HSPs are a group of proteins that are present in cells of all organisms and exist in various forms.

### 2.3.2 Heat shock proteins in laser-based therapeutics

At the cellular level, HSPs exist in the nucleus, cytosol, endoplasmic reticulum, and mitochondria at low levels to respond to everyday stresses within the cell. HSPs are subclassified into families according to their molecular weight (Table 1). Each HSP has many roles and can exist in various locations within the cell. HSPs play important physiological roles in normal conditions and in situations involving both systemic and cellular stresses. HSP expression patterns change when cells are exposed to elevated temperature or other stressors (Snoeckx et al., 2002; Yamasaki et al., 2008). Heat stresses cause several proteins in cells to denature (Chen et al., 2002), and HSPs protect cells by translocating or refolding stress-denatured proteins, thereby preventing aggregation with other proteins in the cell (Wang et al., 2003; Verrico et al., 2001).

HSP promoters are used to control the expression of therapeutic genes in ablative and nonablative laser procedures (Rome et al., 2005). Therefore, temporal evaluation of HSP expression in tissue after laser-based therapeutic procedures can

**TABLE 1:** Heat shock proteins

| HSP family | Members | Intracellular location |
|---|---|---|
| Small PHSs | HSP10, GROES, HSP16, α-crystalin, HSP20, HSP25 | Cytosol |
| HSP40 | HSP40, DNAJ, SIS1 | Cytosol |
| HSP47 | HSP 47 | Endoplasmic retuculum |
| Calreticulin | Calreticulin, Calnexin | Endoplasmic retuculum |
| HSP60 | HSP60, HSP65, GROEL | Cytosol and mitochondria |
| HSP70 | HSP72, HSC70 (HSP73), HSP110/SSE, DNAK, SSC1, SSQ1, ECM10, Grp78 (BiP), Grp170 | Cytosol Mitochondria Endoplasmic reticulum |
| HSP90 | HSC84, HSP86, HTPG Gp96 (Grp94, endoplasmin) | Cytosol Endoplasmic reticulum |
| HSP100 | HSP104, HSP110, CLIP proteins HSP78 | Cytosol Mitochondria |

provide significant information regarding damaged cells and thermally affected tissue surrounding the lesion (Rome et al., 2005; Steel et al., 2004; Boehm et al., 2003). Likewise, HSPs have been shown to correlate with cytoprotective function in cultured cells and with improved healing of damaged tissue in humans and animal models (O'Connell-Rodwell et al., 2008; Sajjadi et al., 2013). Hence, studying the expression of HSPs as reporters of thermal damage and mediators of therapeutic effects to tissues is important in the development of thermal therapies. Investigating the temporal expression patterns of heat shock proteins in response to laser treatment of living tissue will support a better understanding of the effects of laser-induced heating during human therapeutic treatment.

#### *2.3.3 Heat shock protein 70*

HSP70 (molecular weight of 70 kDa) is the best understood among members of the heat shock family of proteins. Its functions include acting as a molecular chaperone facilitating the assembly of proteins, participating in translocation of polypeptides across the cell membrane and to the nucleus, assisting in the folding of nascent polypeptides translated at the ribosome, targeting misfolded and damaged proteins for degradation, dissembling protein aggregates, acting as regulatory molecules in protecting cells from thermal or oxidative proteins, and inhibiting apoptosis (Bukau et al., 2006).

#### *2.3.4 Heat shock protein 47*

HSP47 is a procollagen-specific chaperone whose expression in smooth muscle cells is essential for collagen synthesis. It is expressed constitutively in cells that synthesize collagen and is involved in collagen type I biosynthesis. HSP47 plays a vital role in folding and assembling collagen. Up-regulation of HSP47 following hyperthermia and photodynamic therapy may promote collagen synthesis during the healing process. Thus, it is important to understand HSP expression to better elucidate its role in the course of recovery following laser procedures (Dafforn et al., 2001).

#### *2.3.5 Heat shock protein analysis*

A variety of techniques including Western blotting, enzyme-linked immunosorbant assay (ELISA), and *in situ* hybridization have been used to analyze cellular damage and tissue injury following laser irradiation (Brown et al., 2007) by quantifying HSP expression in tissues. In order to illustrate tissue-level patterns of expression, imaging methods employing confocal microscopy are particularly useful. In two such studies, in vivo induction of HSP70 in transgenic mice (firefly luciferase or green fluorescent protein gene under the control of the HSP70 promoter) was detected by bioluminescence imaging (O'Connell-Rodwell et al., 2008; Brown et al., 2007; Wilmink et al., 2008). In an *in vitro* study, the kinetics of HSP70 expression were measured by quantitative analysis of serial fluorescence images cap-

tured in cultured bovine aortic endothelial cells (BACEs) exposed to heat. This study showed a direct correlation between levels of heat shock protein expression and efficiency of its tissue protection function in BACEs (Wang et al., 2008). The space–time distribution of HSP70 and HSP47 in tissues can also be detected by immunofluorescence labeling of cells or tissues (Brown et al., 2007; Wilmink et al., 2008; Leger et al., 2000, Hawes and Satiat-Jeunemaitre, 2001; Georgala and Boothroyd, 1964; Dams et al., 2010) in which antibodies chemically conjugated with a fluorescent dye are visualized under fluorescence microscope or confocal microscope (Sajjadi et al., 2013).

## 3. LASER ABLATION OF SKIN TISSUE

### 3.1 Thermal Ablation

To study the temperature distribution and analyze the heat diffusion zone during laser irradiation of the skin tissue, the energy equation is coupled with the Fourier heat conduction equation, and the resulting parabolic equation is solved numerically. The numerical models are used to predict the temperature rise at the surface just before the onset of photothermal ablation. A pulse laser beam of pulse width ($t_p$) is incident normally and focused on the sample. The laser beam has a Gaussian distribution in the radial direction and hence an axisymmetric cylindrical coordinate system is used to describe the geometry. The Fourier heat conduction equation is given by

$$q(r, z, t) = -\kappa \nabla T(r, z, t) \ , \tag{1}$$

where $T$ is the temperature, $r$ and $z$ are the spatial coordinates, $t$ is the time, $q$ is the heat flux, $\kappa$ is the thermal conductivity of skin tissue, and $\nabla$ is the gradient. Incorporating scattering and absorption of laser energy in the tissue medium, the energy equation is given as (Sajjadi et al., 2008c; Onyejekwe et al., 2009):

$$-\nabla \cdot q \ (r, z, t) + S = \rho C \frac{\partial T}{\partial t} \ , \tag{2}$$

$$S = k_a I_0 \ \exp\{ -4 \ \ln 2 \times [(t - z / c) / t_p - 1.5]^2 \ \}$$

$$\times \exp \left( \frac{-2r^2}{\sigma^2} \right) \exp \ (-k_e [z - Z(t)]) \quad , \tag{3}$$

where $\rho$ is the density of skin tissue, $C$ is the specific heat of skin tissue, $I_0$ is the maximum intensity of the laser beam at the sample surface, $k_a$ is the absorption coefficient of the skin tissue, $k_e$ is the extinction (scattering and absorption combined) coefficient of the skin tissue, $S$ is the laser source term, $Z(t)$ is the coordinate of the phase separation boundary, and $\sigma$ is the spatial variance of the Gaussian laser beam.

The boundary conditions used are as follows:

(i) all the boundaries except the laser incident surface are insulated,
(ii) at the laser-incident surface free convection heat exchange [e.g., heat transfer coefficient = 10 W/($m^2$·K)] with surrounding ambient air (25°C) can be considered,
(iii) the temperature profile is symmetric about the $z$ axis,
(iv) at the ablation interface, temperature is equal to the vaporization temperature (100°C),
(v) at the ablation interface an additional equation governing $Z(t)$ is obtained by considering an interface energy balance at $z = Z(t)$ involving latent heat of ablation,
(vi) initially ($t = 0$) the temperature is equal to the ambient temperature.

Equations (1)–(3) are discretized and combined to obtain a finite-difference equation to be solved using an Alternating Direction Implicit (ADI) scheme with Backward in Time and Central in Space (BTCS). Details of this discretization scheme and Van Neumann stability analysis can be found in the literature (Sajjadi et al., 2008a; Tanehill et al., 1984). The solution is obtained by using the values of $\Delta r$ and $\Delta z$ equal to $1.5625\cdot10^{-4}$ m and $2.5\cdot10^{-5}$ m, respectively, and $\Delta t = 0.05\cdot10^{-12}$ s. The resultant finite difference equation is solved by the Tri-Diagonal Matrix Algorithm (TDMA).

In Eq. (3) of the above model, radiation heat transfer is simply treated via the Beer–Lambda law. As we know, however, biological tissues are highly scattering and weakly absorbing as concerns the laser light. Therefore, a radiative transfer modeling would provide much better prediction of the laser energy distribution and propagation inside the tissue. For circular laser beams, the diffuse radiation intensity $I_l^d$ in a discrete ordinate $\vec{s}_l$ is described by the time-dependent equation of radiative transfer in cylindrical coordinates:

$$\frac{1}{c}\frac{\partial I_l^d}{\partial t}+\frac{\mu_l}{r}\frac{\partial}{\partial r}(rI_l^d)-\frac{1}{r}\frac{\partial}{\partial \phi}(\eta_l I_l^d)+\xi_l\frac{\partial I_l^d}{\partial z}+k_e I_l^d = k_e S_l,\ l=1,2,....,M, \tag{4}$$

where $\mu_l$, $\eta_l$, and $\xi_l$ are the three directional cosines, $c$ is the speed of light in the medium, and $S_l$ is the radiative source term, which is

$$S_l=(1-\omega)I_b+\frac{\omega}{4\pi}\sum_{j=1}^{M} w_j\Phi_{jl}I_l^d+S_b^l, \tag{5}$$

where $I_b$ the blackbody emitting intensity of tissue, $\omega = k_s/k_e$ is the scattering albedo, $w_j$ is the appropriate angular weight in discrete direction $\vec{s}_j$, $\Phi_{jl}$ represents the scattering phase function $\Phi$ ($\vec{s}_j \rightarrow \vec{s}_l$), and $S_b^l$ is the source contribution of the laser irradiation and can be expressed as

$$S_b^l = \frac{1}{4\pi}I^b\Phi\ (\vec{s_b} \rightarrow \vec{s}_l) \tag{6}$$

in which the unit vector $\vec{s}_l$ represents the laser incident direction and $I^b$ is the ballistic radiation (i.e., the laser incident heat flux).

Kim and Guo (2004) provided a detailed solution to the above radiative heat transfer model with appropriate boundary conditions. This model can treat both steady-state and ultrafast radiation. Recently, Jiao and Guo (2009) applied this model to focused laser beam interaction with skin tissues; and Hunter and Guo (2012a,b) introduced a new normalization technique for treating anisotropic scattering of light in biological tissues. Guo and Hunter (2013) will also provide a comprehensive review on this topic in the same issue; and thus, the details are not repeated here.

### 3.2 Plasma-Mediated Ablation

Plasma-mediated ablation, also known as laser-induced optical breakdown, has been described as the interaction of a strong electromagnetic field with electrons in a condensed medium, which can lead to the generation of free electrons in the conduction band through multiphoton or tunnel ionization (Kennedy, 1995). These free charges can subsequently gain sufficient kinetic energy from the electric field by inverse Bremsstrahlung absorption (IBA) to produce more free electrons via avalanche ionization (Kennedy et al., 1995). The rapid ionization of the medium leads to plasma formation and a drastic increase of the absorption coefficient that in turn gives rise to a rapid energy transfer from the radiation field to the material. For ablation of biological tissues, multiphoton ionization is most likely the pathway for generating seed electrons for avalanche ionization. Another possibility is the chromophore ionization pathway in generating free electrons due to adiabatic heating of chromophores in biological tissues.

The time evolution of the free-electron density in a control volume can be described by a rate equation in a generic form:

$$\frac{\partial \rho}{\partial t} = \left(\frac{\partial \rho}{\partial t}\right)_{mp} + \left(\frac{\partial \rho}{\partial t}\right)_{ch} + \eta_{ava}\rho - \eta_{diff}\rho - \eta_{rec}\rho^2, \tag{7}$$

where the free-electron density $\rho$ is a function of time. The first three terms on the right-hand side represent the production of free electrons through multiphoton, chromophore, and avalanche ionizations, respectively. The last two terms are the electron losses through diffusion and recombination, respectively. The avalanche ionization rate and the diffusion rate are proportional to the number of the existing free electrons. The recombination rate is proportional to $\rho^2$, as it involves an interaction between two charged particles (an electron–hole pair). Jiao and Guo (2011) found that the chromophore effect is actually negligible for skin tissues.

#### *3.2.1 Multiphoton ionization*

To ionize an atom or molecule with ionization energy, the number of photons required is

$$k = \left\langle \Delta E / (\hbar\omega) + 1 \right\rangle,$$

in which $\hbar$ is the reduced Planck constant and $\omega = 2\pi c/\lambda$ is the laser circular frequency. An approximate expression for the multiphoton ionization rate is derived as (Kennedy, 1995)

$$\left(\frac{\partial \rho}{\partial t}\right)_{mp} \approx \frac{2\omega}{9\pi}\left(\frac{m'\omega}{\hbar}\right)^{3/2}\left[\frac{e^2}{16m'\Delta E\omega^2 c\varepsilon_0 n} I^b\right]^k \times \exp(2k)\varphi\left(\sqrt{2k - \frac{2\Delta E}{\hbar\omega}}\right), \tag{8}$$

where an electron charge is $e = 1.6022 \cdot 10^{-19}$ C, $m'(= m/2)$ is the reduced excitation mass, in which $m$ is the mass of electron, $n$ is the refractive index, $\varepsilon_0$ is the vacuum permittivity, and $\varphi(x)$ expresses the Dawson function.

### 3.2.2 Avalanche ionization

As soon as a free electron exists in the interaction volume, it gains energy from the electric field through IBA of photons and can generate further free electrons through impact ionization. Conservation of momentum requires that the absorption of photons from the laser pulse take place during collisions of the free electrons with the surrounding molecules. The avalanche ionization rate coefficient $\eta_{ava}$ derived by Kennedy et al. (1995) for ocular and aqueous medium is given by

$$\eta_{ava} = \frac{1}{\omega^2\tau^2 + 1}\left(\frac{e^2\tau}{c\varepsilon_0 n m \Delta E} I^b - \frac{m\omega^2\tau}{M_m}\right). \tag{9}$$

Here, $\tau \approx 1.7$ fs is the time of collision between an electron and a heavy particle (Sun et al., 2005) and $M_m$ is the mass of molecule.

### 3.2.3 Diffusion and recombination

The diffusion of electrons from the focal volume was estimated by approximating the focal volume as a cylinder of radius $w_{0R}$ and length $z_R$. Thus, the diffusion rate per electron is expressed as (Noack and Vogel, 1999)

$$g = \frac{\tau\Delta E}{3m}\left[\left(\frac{2.4}{w_{0R}}\right)^2 + \left(\frac{1}{z_R}\right)^2\right]. \tag{10}$$

The recombination rate $\eta_{rec}$ is considered as $2 \cdot 10^{-9}$ cm$^3$/s (Docchio, 1988).

The critical free-electron density is used to be estimated in the orders of $10^{18}$–$10^{20}$ cm$^{-3}$. Theoretically, the upper limit of free-electron density is given by the requirement that the plasma frequency, $\omega_p = \sqrt{e^2\rho/m_e\varepsilon_0}$, must remain below the light frequency $\omega$ in order to effectively couple energy into the plasma. At electron densities greater than $\rho = \omega^2 m\varepsilon_0/e^2$, the plasma becomes highly reflective, and the incoming laser light leads to growth of the plasma volume rather than the

free-electron number (Noack and Vogel, 1999). Therefore, the critical free-electron density for plasma-mediated ablation is calculated by $\rho_{cr} = \omega^2 m\varepsilon_0/e^2$ (Vogel et al., 2005).

## 4. EXPERIMENTAL METHOD

### 4.1 Experimental Method for Laser Ablation of Skin Tissue

The schematic of the experimental setup is shown in Fig. 1. A 1552-nm desktop diode laser (Raydiance Inc.) operating at a wavelength of 1552 nm and having a temporal pulse width (tp) of 1.3 ps (FWHM) is used in this experiment. The array of time-averaged power values that can be produced by the laser varies from 0.17 W to 2.50 W through the adjustment of both the energy per pulse which varies from 1–5 μJ/pulse and the repetition frequency which varies between 25 kHz and 500 kHz.

The beam is focused using a high-power 20× microscope objective which focuses the beam to a spot diameter of approximately 10 μm for a focal length of 21 mm. Due to losses through the mirrors and objective lens, the power on the samples varies from 0.07 W to 1.48 W. During the experiment the laser time-averaged power is constantly monitored using a power meter. The samples are well insulated on all sides (except on the irradiated face) to prevent heat loss to the surroundings. A thermal imaging camera (IR Flexcam Pro, Infrared Solutions) is used to record the radial surface temperature profile of samples. The images are recorded with a computerized data acquisition system and processed with National Instruments IMAQ Vision Builder Image processing software. The camera provides a measurement range of 0°C to 350°C with a sensitivity of ±0.09°C at 30°C. The spectral response of the camera is 8 to 14 μm. Experiments are conducted

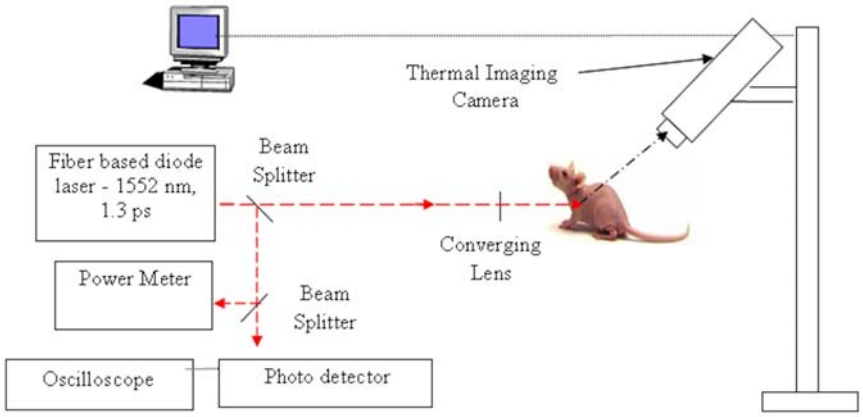


**FIG. 1:** Schematic of the experimental setup for laser irradiation using a focused beam of a 1552-nm pulse laser with 1.3-ps pulse width

with freshly excised skin tissue samples having thicknesses of 2–3 mm obtained from mice using 1552-nm diode laser. After irradiating the tissue samples with the laser, histological analysis is performed to analyze the heat-affected zone produced by laser irradiation. The frozen sectioning technique is used for histological studies. The resolution provided by the frozen section technique is sufficient to observe thermal damage in the tissue caused by laser irradiation. In this technique, the ablated portion of the tissue is cut along with some surrounding nonirradiated tissue right after the ablation and embedded in the cryomold made of OCT (Optimal Cutting Temperature) compound. Then sections of thickness 20 μm are cut using cryostat. The temperature inside the cryostat is maintained at $-24^{o}$C during sectioning. The sections are stained using hematoxylin and eosin (H&E) stain, which is a rapid staining method that is commonly used due to its simplicity. This progressive stain creates stained sections, which have deep blue nuclei with a pink or rose-colored background of other cytoplasmic structures. Once the sample preparation is complete, slides are viewed under an optical microscope using 40× magnification. Tissue samples are translated in a direction perpendicular to the laser beam using three-axis automated Newport SMC 100 motion-controlled stages interfaced with National Instruments Lab view 8.0 to run the controllers. The maximum velocity of these controllers is 25 mm/sec and can be varied in steps of 50 μm/s. Scanning of the tissue sample ensures a fresh region of the tissue to be always exposed to laser pulses. For the case of zero scanning velocity, tissue samples are irradiated at the same spot for finite time duration. The ablation depth and width is measured using image-processing software (Scandium) in order to correlate ablation depth to laser parameters. The software is calibrated to provide measurements in millimeters corresponding to the magnification at which an image is captured. In this way, laser-induced damage dimensions are calculated for a particular set of laser parameters.

### 4.2 Experimental Method for Ablation of Subcutaneous Tumors

A focused beam from an ultrashort pulse 1552-nm laser is used to ablate subcutaneous tumors with minimal thermal damage to surrounding healthy tissues. Longer-wavelength infrared lasers have been used for biomedical applications involving human tissues. For example, 1700-nm femtosecond lasers have been used to produce subsurface incisions in human sclera (Sacks et al., 2001), and a 1552-nm femtosecond laser generated surface lesions in human dermis via plasma-mediated ablation without any alternation in tissue morphology (Huang and Guo, 2009). Nonablative fractional photothermolysis is currently approved by the US Food and Drug Administration (FDA) for the treatment of pigmented lesions, periorbital rhytides, skin resurfacing, melasma and soft tissue coagulation, acne and surgical scars, and actinic keratoses (Allemann and Kaufman, 2010). A wavelength of 1550 nm is ideal for fractional resurfacing, allowing sufficient penetration into tissue (Thongsima et al., 2010; Helbig et al., 2010). At higher absorption coeffi-

cients, which is dependent on wavelength, e.g., at 1440 nm, the beam penetrates superficially, providing less volume of tissue treated and ultimately reducing the amount of tissue affected by the collagen remodeling process. The ultrashort pulse laser of 1552-nm wavelength is a relatively new development, and was conceived as an optimal compromise between the effects of optical scatter and optical absorption in silica-based fiber optics for industrial applications. That is, at longer wavelengths optical absorption increases and at shorter wavelengths optical scatter increases at fiber defects. A wavelength of 1550 nm represents the best compromise that produces the lowest absorption and the lowest scatter (Sajjadi et al., 2011a). In addition, lasers with wavelengths above 1400 nm (and particularly noncollimated beams) are relatively eye-safe because their output is not readily transmitted through the cornea. Finally, because the threshold for plasma optical breakdown, and therefore ablation threshold, decreases with increasing tissue absorbance for subnanosecond pulses (Oraevsky et al., 1996) and because biological tissue exhibits significant absorbance at this wavelength, the 1552-nm wavelength may provide a novel mechanism for therapeutic ablation, particularly when delivered via fiber optics. Therefore, the goal of the work presented here was to determine the efficacy of focused-beam 1552-nm ultrashort pulsed laser for subcutaneous tumor ablation.

In order to demonstrate subcutaneous ablation using a focusing beam and to select optimal laser parameters for tissue ablation, we performed experiments on normal (without tumor) anesthesized mice. The radial heat spread at the skin surface was measured using a thermal camera, and subsurface radial heat spread was measured using needle-type thermocouples. Once the efficacy of this technique was demonstrated, experiments were performed on anesthesized mice with mammary tumors. During tumor ablation experiments, temperatures at the surface and at the subsurface tumor locations were monitored continuously. To minimize temperature rise and for complete tumor ablation, scanning of the laser across the tumor area and its margin was performed by mounting samples on a computerized translation stage and moving them within the focal plane of the beam. After ablation, the extent of plasma-mediated ablation and thermal damage was studied using histology to demonstrate focal ablation without apparent damage to surrounding epidermal and dermal layers.

*In vivo* experiments were first performed on anesthesized healthy mice (available in-house from animal facilities in Biological Sciences Department) to observe the effectiveness of achieving the desired ablation volume and temperature rise at the subsurface location using a focused laser beam. Experiments were performed *in vivo* on anesthesized mice with mammary tumors in order to demonstrate the therapeutic effect of this novel tumor irradiation technique. Tumor mice used in this study were of the inbred strain FVB/N-Tg (MMTVneu) 202Mul/J, purchased from the Jackson Laboratories (Bar Harbor, ME, USA). These mice contain a mammary tumor virus (MMTVneu) transgene, expressed in mammary tissue, salivary gland, and lung. Mice were purchased as retired breeders containing focal

metastatic tumors in the mammary glands. The tumors utilized in this study had a diameter of 1–3 mm at a depth of 1–3 mm from the surface. Mice were anesthesized using sodium pentobarbital delivered I.P. at a dose of 90 mg/kg before performing laser irradiation experiments. Because tumor dimensions were larger than the damage produced by the laser beam focused at a single spot, the mouse was translated in the focal plane during the experiment for complete ablation of tumor and its margin area. After completion of the experiments, mice were allowed to recover before being reintroduced to the animal colony. However, some mice were sacrificed after the experiment to perform histological studies in order to observe the damage produced by laser irradiation. All experimental procedures on mice were approved by Florida Tech's Institutional Animal Care and Use Committee (IACUC).

## 4.3 Characterization of Ablated Tissue

### *4.3.1 Thermal imaging camera*

A thermal imaging camera (IR Flexcam Pro, Infrared Solutions, Everett, WA) was used to record the radial surface temperature profile of the samples. Images were recorded with a computerized data acquisition system and processed with National Instruments IMAQ Vision Builder image processing software. The camera provides a measurement range of $0^{o}$C to $350^{o}$C with a sensitivity of $\pm 0.09^{o}$C at $30^{o}$C and spectral response range of 8 to 14 μm. For subsurface temperature measurement, temperature was recorded using a needle type thermocouple and computerized data acquisition system running Labview Software. These thermocouples provided a maximum possible measurement range of 0–$480^{o}$C with a sensitivity of $\pm 1^{o}$C and 0.2 s response time.

### *4.3.2 Frozen sectioning technique*

The tissue sectioning protocols for histological and immunohistochemical studies are as follows:

- The region of laser treatment (ablated portion of the tissue along with some surrounding nonirradiated tissue) was dissected immediately following laser treatment.
- Tissue is embedded in OCT (Optimal Cutting Temperature) compound.
- Frozen sections of 20 μm thickness were cut at $-24^{o}$C using cryostat (Leica CM1850) and embedded on the gel coated slides.

### *4.3.3 Histology*

Histological studies (Chung and Mazur, 2009; Loesel et al., 1996, 1998; Fischer et al., 1997) utilizing frozen sectioning technique (Vogel et al., 1998) are performed to analyze the damage zone produced by laser irradiation. The samples are stained in order to more easily distinguish among the different tissue structures. Applica-

tion of hematoxylin and eosin (H&E) is a rapid staining method that is commonly used due to its simplicity. The procedure for preparation of the hematoxylin is described in (Presnell and Schreibman, 1997).

The H&E staining procedure is as follows:

- Cryosections are stained using hematoxylin and eosin (H&E).
- Sections are viewed using a Zeiss Axioskop compound light microscope, and photographed using a Penguin CL-600 digital camera.
- Ablation depth and width were determined using image processing software (Scandium) after calibration of the microscope and objectives. The software was calibrated to provide measurements in millimeters corresponding to the pixel values of the images. In this way, laser-induced damage zone dimensions were calculated for a particular set of laser parameters.

#### *4.3.4 Immunohistochemistry*

Immunohistochemistry is performed to localize HSP70 and HSP47 at the lesion site over the course of time following laser irradiation. Cryosections are fixed in Zamboni's solution. Sections then are labeled with antisera specific for HSP70 (mouse polyclonal IgG anti-HSP70) at 1:1000 dilution and HSP47 (mouse polyclonal IgG anti-HSP47) at 1:1000 dilution (primary and secondary antisera purchased from Santa Cruz Biotechnology, Inc.). Sections are then treated with secondary antisera conjugated to either Alexa 555 (emission maximum at 555 nm) conjugated to anti-mouse IgG for labeling of HSP70, or Alexa 488 (emission maximum at 488 nm) conjugated to anti-rabbit IgG for HSP47. To visualize overall tissue architecture, cell nuclei are labeled using the florescent DNA-binding dye DAPI (emission maximum 461 nm). A Nikon C1Si laser scanning confocal microscope is used to visualize the extent of expression of HSPs.

## 5. RESULTS AND DISCUSSION

### 5.1 Selection of Laser Parameters

Laser-based surgery has traditionally relied upon continuous-wave lasers. It has been demonstrated (Sajjadi et al., 2011a, 2013) that the focused beam of a short-pulse laser can produce precise lesions with less thermal effects in the surrounding healthy tissue. Figure 2 illustrates the histology of ablated tissue immediately after irradiation. Short-pulse laser produces precise and clean lesion with a smaller heat-affected region in surrounding tissue (Fig. 2a). Continuous laser, however, produced a dramatic color change in hematoxylin and eosin (H&E) — stained tissues around the site of a focal lesion (Fig. 2b) which suggests that thermally denatured collagen in the skin surrounding the focal lesion is found some distance away from the lesion site. Thus, immediately after ablation, the extent of damage is much larger when ablation is performed using continuous-wave laser beam than when using a short-pulse laser.

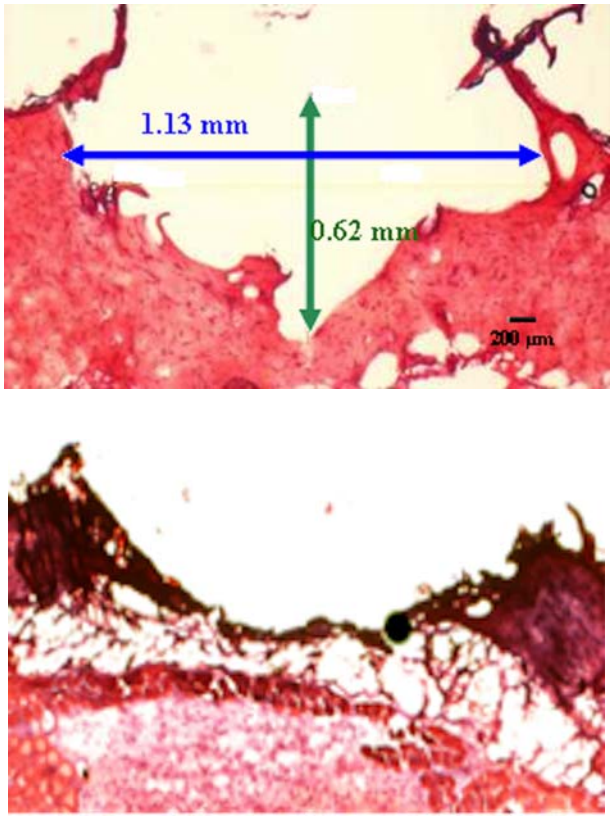


**FIG. 2:** Histological section of freshly excised mouse skin tissue immediately after laser ablation using either a short-pulse laser (a) or a continuous-wave laser (b) [reproduced from (Sajjadi et al., 2013]

This conclusion was confirmed by measuring temperature distribution with a thermal camera during laser irradiation. The maximum temperature rise varies between 30 and 34°C for short-pulse laser and between 40 and 45°C for continuous laser beam (data not shown). The rate of temperature rise, maximum temperature, and thermal heat spread for a short time interval after laser irradiation are all higher when irradiation is done with a CW laser than when using a short-pulse laser (Sajjadi et al., 2011a).

Temperature distribution before the onset of ablation has been obtained experimentally and numerically for the case of tissue medium irradiated using an ultrashort pulse laser. Parametric studies are performed to observe the effects of repetition rate, time-average power, and scanning velocity on the surface peak temperature rise and radial heat spread.

Experiments are performed on tissue samples for the following laser parameters: repetition rate = 500 kHz, pulse width = 1.3 ps, time-average power = 1.48 W,

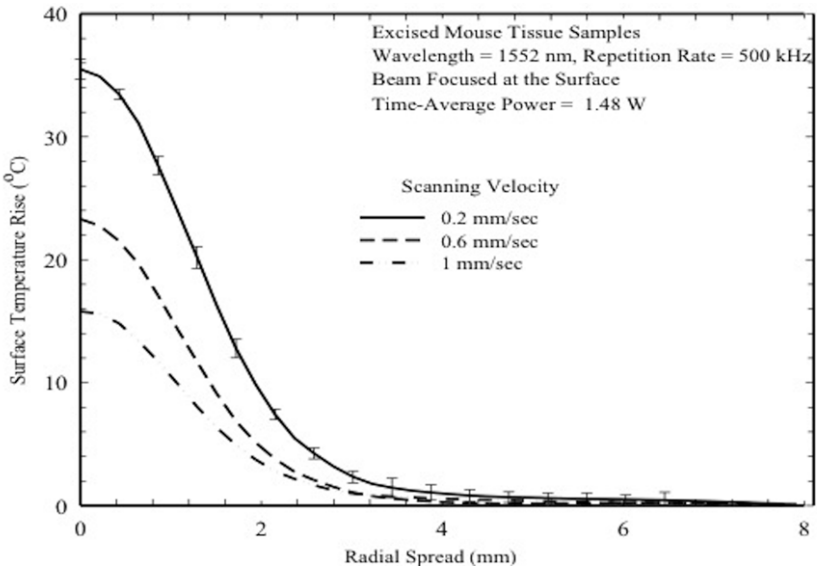


**FIG. 3:** Radial temperature distributions for different scanning velocities

and energy per pulse = 5 μJ/pulse. The tissue samples are scanned at different velocities. Figure 3 shows the radial temperature distribution for scanning velocity ranging from 0.2 mm/s to 1 mm/s. It is observed that the peak temperature increases with decreasing scanning velocity. The rises in temperatures for the case of slow scanning velocities are significantly higher than those for faster scanning velocities. Slower scanning rates result in a greater density of pulses that are incident upon the sample leading to higher amounts of laser energy deposition which manifests as high peak temperatures. The error bars plotted in Fig. 3 represent uncertainty in experimental measurements for the case of scanning velocity equal to 0.2 mm/s. Uncertainty for other scanning velocities are in the same order and is not shown. Considering a 99% confidence interval, the precision index for a total of three runs is calculated. The standard deviation between the three runs at each individual nodal point is evaluated. Thus, the total uncertainty value at each nodal point is the product of the precision index times the standard deviation. For example, for the case of scanning velocity of 0.2 mm/s, the maximum uncertainty in temperature measurement is $0.89^{o}$C.

Figures 4a,b show the radial temperature distribution before onset of ablation of tissue sample for different laser repetition rates and time-average powers for the case of zero scanning velocity (which corresponds to spot irradiation). The samples are irradiated for a finite time and data is represented for two exposure times- 5 s and 10 s. Mathematical modeling of the transient heat conduction equation is used to predict the surface temperature rise and the ablation depth. Comparison of the peak temperature rise between experimental measurements and numerical mod-

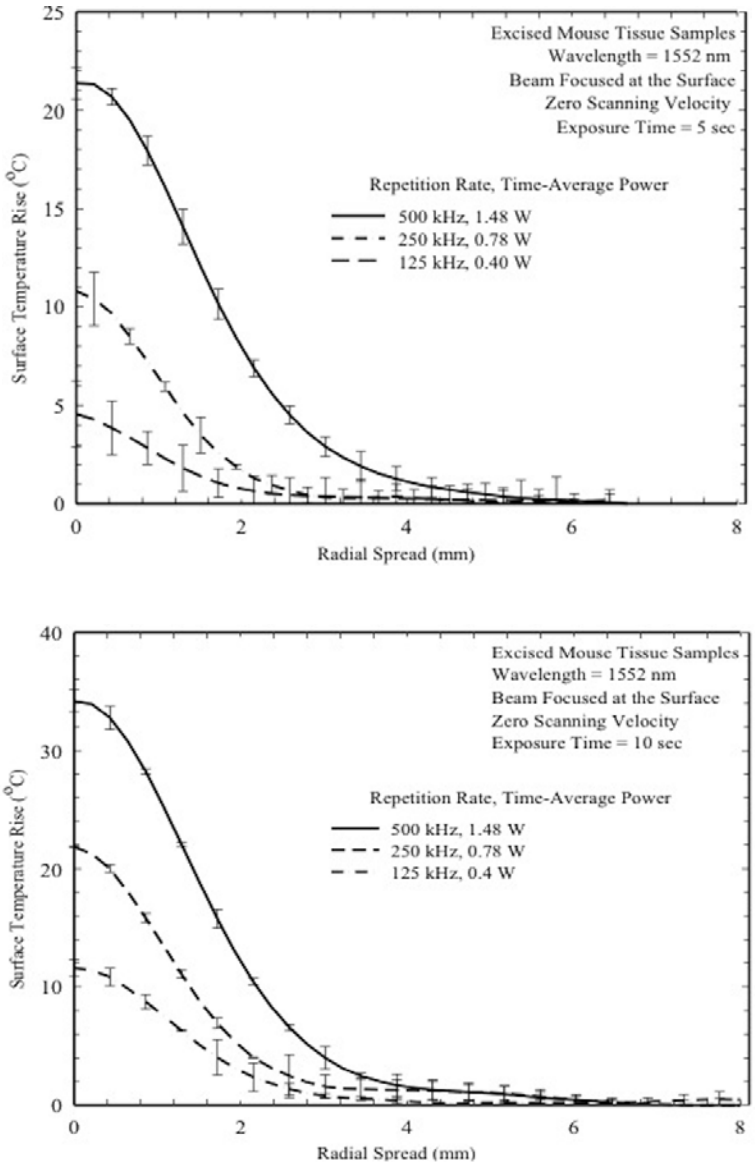


**FIG. 4:** Radial temperature distribution for different time-average power having exposure time of (a) 5 s (a) and 10 s (b)

els for different laser parameters and exposure time is shown in Fig. 5 for the case of zero scanning velocity. It is evident from Fig. 5 that the peak surface temperatures obtained in experimental measurements and modeling are in very good agreement.

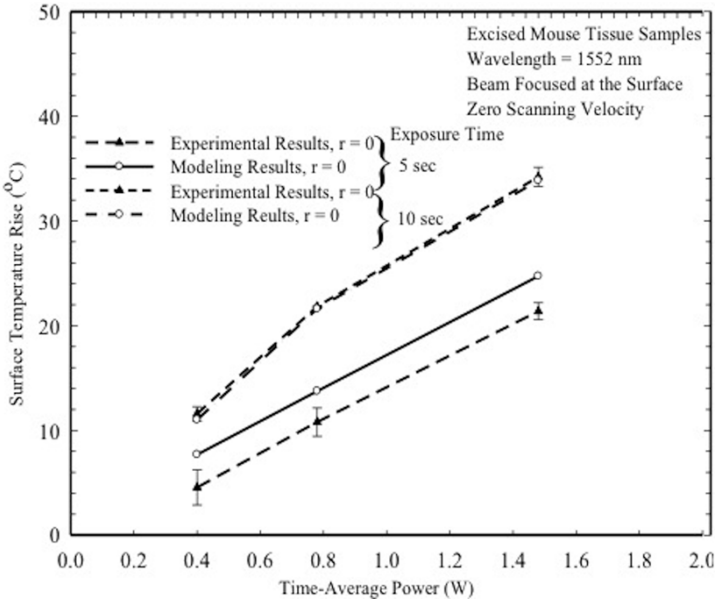


**FIG. 5:** Comparison between numerical model and experimental results for the surface temperature rise as a function of time-averaged power

### 5.2 Ablation of Subcutaneous Tumors

The results show that an ultrashort pulse 1552-nm laser, focused beneath the epidermal surface, can produce precise ablation of a tumor with minimal effects on the surrounding healthy tissue. Initially, parametric studies were performed on anesthesized healthy mice to select optimal laser parameters including the pulse repetition rate, time-averaged power, and scanning velocity with respect to temperature rise and radial heat spread in tissues. Experiments were performed for different time-averaged laser powers and repetition rates, keeping the energy/pulse constant, and each experiment was performed at least three times for each set of laser parameters to ensure repeatability and to calculate measurement uncertainty. The skin ablation threshold was calculated as $9.14 \pm 1.43$ J·cm$^{-2}$ (Huang and Guo, 2010). In all initial experiments, no significant ablation occurred below the time-averaged laser power of 1.48 W and repetition rate of 500 kHz. Therefore, these laser parameters were used for all subsequent experiments.

To assess the effectiveness of ablation at subsurface locations, experiments were performed on anesthesized normal mice by focusing the laser at 1 mm underneath the skin surface. Histological examination of mouse skin tissue (Fig. 6) shows that laser irradiation produces a focal lesion that does not compromise tissue external to the lesion location (compare Fig. 6b, irradiated, with Fig. 6a, nonirradiated). The color change of the hematoxylin and eosin stain to deep pink suggests that

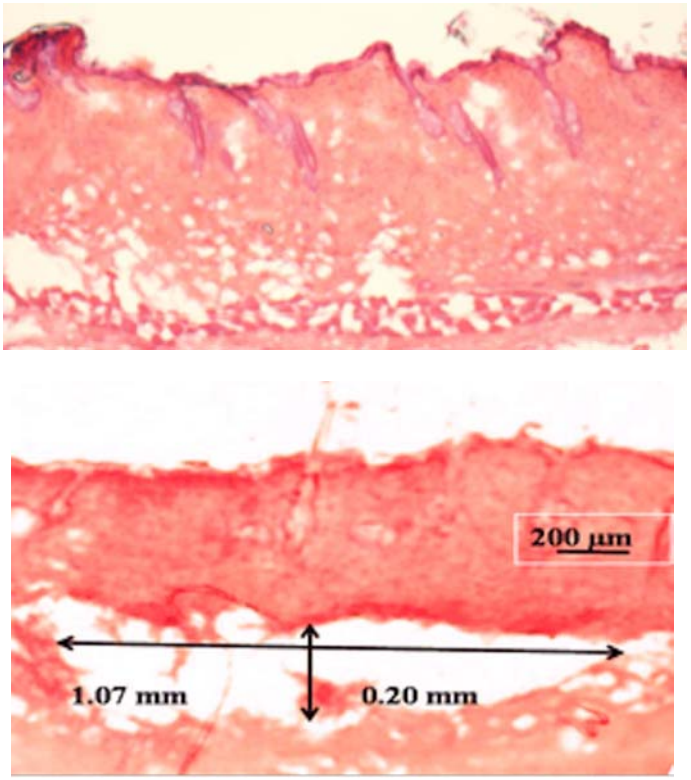


**FIG. 6:** Histology of freshly excised tissue from an anesthesized mouse: a) nonirradiated; b) immediately after laser irradiation using 1552-nm ultrashort pulse laser focused beneath the surface of the skin [reproduced from (Sajjadi et al., 2011a)]

the lesion may be produced by thermal denaturation of collagen present in the skin (Fig. 6b).

Application of successive laser pulses at the same spot can cause significant thermal damage to surrounding tissue. Therefore, in order to overcome the problems associated with accumulation of successive laser energy pulses at the same spot during laser irradiation, samples were translated within the focal plane of the laser beam. Figure 2a shows that without lateral translation of the laser relative to the sample (i.e., translation rate of 0.0 mm/s), a significant zone of damage was produced in Fig. 3, the laser was focused very near the surface of the sample). However, lateral translation of the sample at 1.0 mm/s produces a significantly smaller zone of ablation (Fig. 7). Thus, the size of the lesion increases with increasing exposure time. Figure 7 also demonstrates that the focused 1552-nm ultrashort pulse laser produces ablation volumes with crisp edges and little collateral thermal damage to nontargeted adjacent tissue. After observing the effectiveness of the focused 1552-nm laser for producing precise subsurface ablation, and demon-

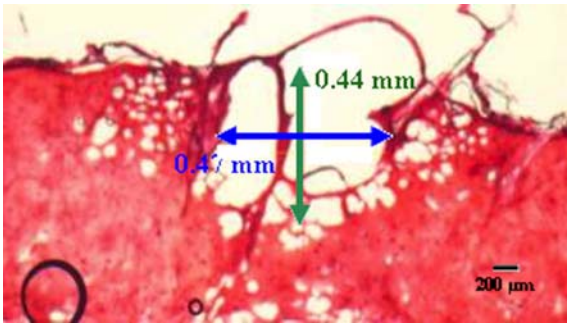


**FIG. 7:** Histological analysis of laser irradiation when the beam of 1552-nm ultrashort pulse laser is focused at the skin surface showing that lesion size depends upon the scanning rate. Scanning velocity = 1.0 mm/s [reproduced from (Sajjadi et al., 2009)]

strating the effect of scanning velocity on lesion size, experiments were performed on anesthesized mice with mammary tumors. In order to understand the time course of temperature effects of a subsurface-focused beam, a needle-type thermocouple was located approximately 2 mm from the laser focal point to measure temperature below the surface.

An infrared camera was used to monitor temperature at the surface. Figure 8 shows that the rate of temperature increase is greater at the tumor location than at

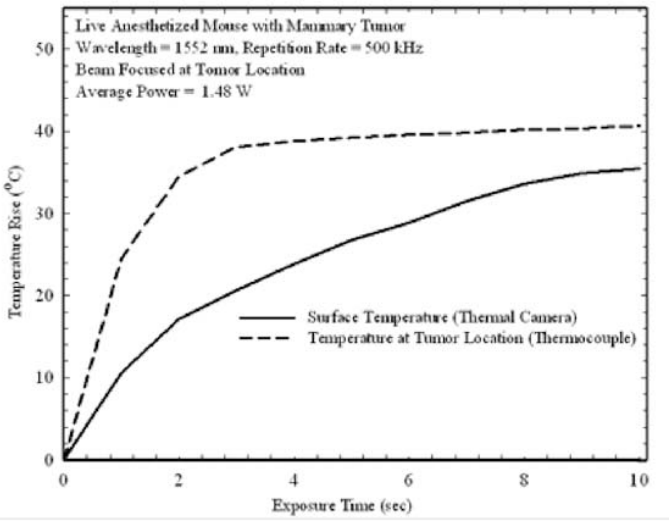


**FIG. 8:** Temperature rise at the skin surface and at the subsurface tumor location in an anesthesized FVB/N-Tg (MMTVneu) 202 Mul/J mouse with mammary tumor. The beam of 1552-nm USP laser was focused at the subsurface tumor location (2-mm deep to the epidermal surface) [reproduced from (Sajjadi et al., 2011a)]

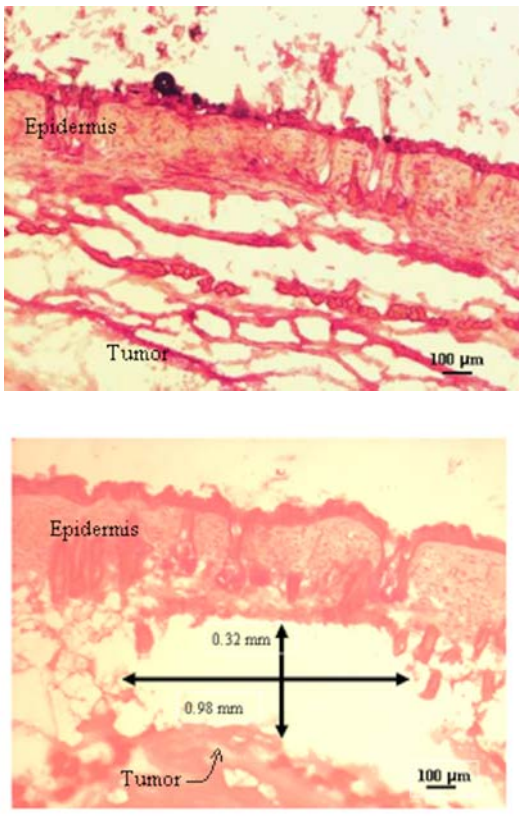


**FIG. 9:** Histological analysis of normal mouse tissue, and tissue from FVB/N-Tg (MMTVneu) 202 Mul/J at the site of a subsurface tumor: a): freshly excised normal tissue from an anesthesized mouse; b) example of a lesion in FVB/N-Tg (MMTVneu) mouse using subsurface focused 1552-nm laser. Stimulation parameters: scanning velocity = 0.2 mm/s; repetition rate = 500 kHz; time-averaged power = 1.48 W [reproduced from (Sajjadi et al., 2011a)]

the surface, demonstrating that the beam was tightly focused at the tumor site. Because of heat diffusion over the course of long exposure times, the temperature gradient between the tumor location and surface was lower at longer exposure times but over the course of this experiment, temperature was always greater at the lesion site than at the surface (Fig. 8).

Irradiation of tumors with a subsurface-focused ultrashort pulse laser produces results similar to those produced in normal mouse tissue (see Fig. 6). When irradiated in a stationary manner (scanning velocity = 0.0 mm/s), tumor tissue was effectively ablated and the epidermal surface remained intact (Fig. 9a), but the lesion margins appear to exhibit thermal coagulation as would be expected given

the dramatic temperature rise that irradiation produces (see Fig. 5). However, even at the lowest scanning velocity tested, 0.2 mm/s, ablation occurred with clean margins (Fig. 9b), suggesting that the thermal effects were minimal and ablation occurred in a plasma-mediated manner. Thus, complete ablation of tumor tissue with minimal collateral damage depends upon the dose of energy delivered at a given location, which in turn depends upon scanning rate (i.e., the number of repetitive pulses accumulated on the same spot). This result demonstrates that the focusing technique can be used effectively for ablation of subsurface tumors, and optimal scanning velocity can be utilized to produce minimal heat spread and therefore minimal collateral damage.

### 5.3 Expression of Heat Shock Proteins 70 and 47 in Tissues

In order to provide another measure of the extent of thermal effects following laser irradiation, the kinetic expression of HSP70 and HSP47 as indicators of damage and healing procedure at various times following laser injury to the skin was examined. Figure 10a shows a cross section of nonirradiated skin tissue (control),

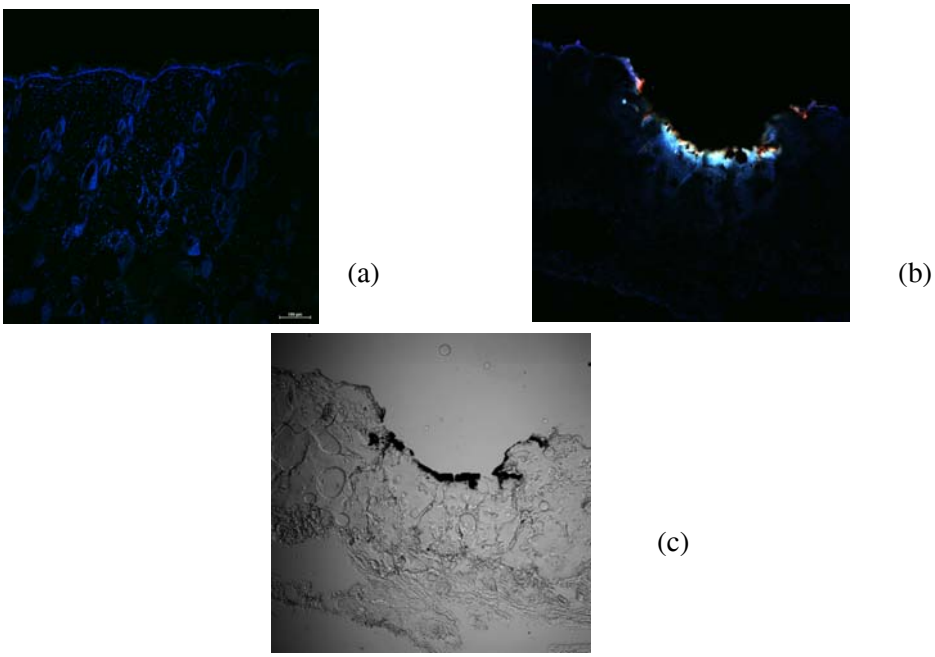


**FIG. 10:** Confocal microscopy of immunolabeled cross sections of mouse skin section immediately after irradiation (time 0). DNA is labeled with DAPI (blue); HSP70 is immunolabeled to appear red; HSP47 is immunolabeled to appear green. Nonirradiated skin tissue (a); laser-irradiated skin tissue (b); visible light image (c). Energy per pulse = 1.5 mJ, pulse width = 200 ns [reproduced from (Sajjadi et al., 2013)

and Fig. 10b shows the cross section of irradiated skin tissue labeled with DAPI and visualized with confocal microscope immediately after irradiation. Confocal images show that the ablated region of the skin exhibits significant autoflorescence. The damage to the cells in skin tissue may cause alterations in the structure of the tissue such that the damaged region emits light across a broad range of wavelengths under laser-scanning confocal imaging. The dark area of the lesion visible in a phase contrast image (Fig. 10c) demonstrates thermally induced damage in the tissue.

To compare the effects of short-pulse versus CW laser, we used an Nd:YAG (1064 nm) laser capable of being operated in either CW or pulsed mode. When this laser is set to a continuous mode, the measured average power is 4.45 W. When the pulse duration is set to 200 ns, the measured energy per pulse is 1.5 mJ. The expression pattern of HSPs in tissue sections irradiated by CW and short-pulse laser were compared at 24 h following laser irradiation (Fig. 11). When used in the CW mode, the laser induced HSP47 expression over a broad area surrounding the lesion, in the tissue immediately surrounding the ablation crater (Figs. 11a,b), and also at distances of up to 0.6 mm away from the site of visibly obvious laser-induced damage (i.e., the damage crater). However, following short-pulse laser irradiation, we show that HSP47 expression was observed only over a much more restricted zone immediately surrounding the ablation crater (Figs. 11c–f). Overall, the level of HSP47 expression appeared lower in tissue exposed to pulse laser irradiation than in tissue exposed to CW laser irradiation.

The time course of HSP70 and HSP47 expression caused by short-pulse laser irradiation was studied by assessing the distribution and intensity of HSP immunolabeling in tissue at 2-, 4-, 6-, 8-, and 24-h post-irradiation. At time 0, no HSP-like immunoreactivity was observed by confocal microscopy, but at 2-h post-irradiation, both HSP47 and HSP70 were apparent (Fig. 12a). At 2-h post-irradiation, HSP70 labeling was abundant in the area immediately surrounding the lesion (Fig. 12b), and the intensity of HSP70 apparently peak at 4-h post-irradiation, at which time its labeling pattern is more scattered in the tissue. HSP47 shows a similar pattern of expression, first noticeable at 2 h, rising over the course of time to peak at 4-h post-irradiation where it is highly localized immediately adjacent to the lesion. At 8-h post-irradiation both HSP70 and HSP47 are present surrounding the lesion and also scattered distant from the lesion (Fig. 12c).

Finally, HSP expression was used as a tool to analyze the extent of damage induced by a focused-beam short-pulse laser when it is tightly focused at a subsurface location. Visible light analysis at 24-h post-irradiation (Fig. 13) shows a lesion fully contained within the dermis. The overlying epidermis was not damaged; tissue was removed only at the focal point of the laser. Confocal microscopy shows a significant amount of HSP47 immunolabeling in the dermis and epidermis above, lateral to, and below the obvious lesion, but very little HSP70 at 24-h post-irradiation under these conditions (Fig. 13).

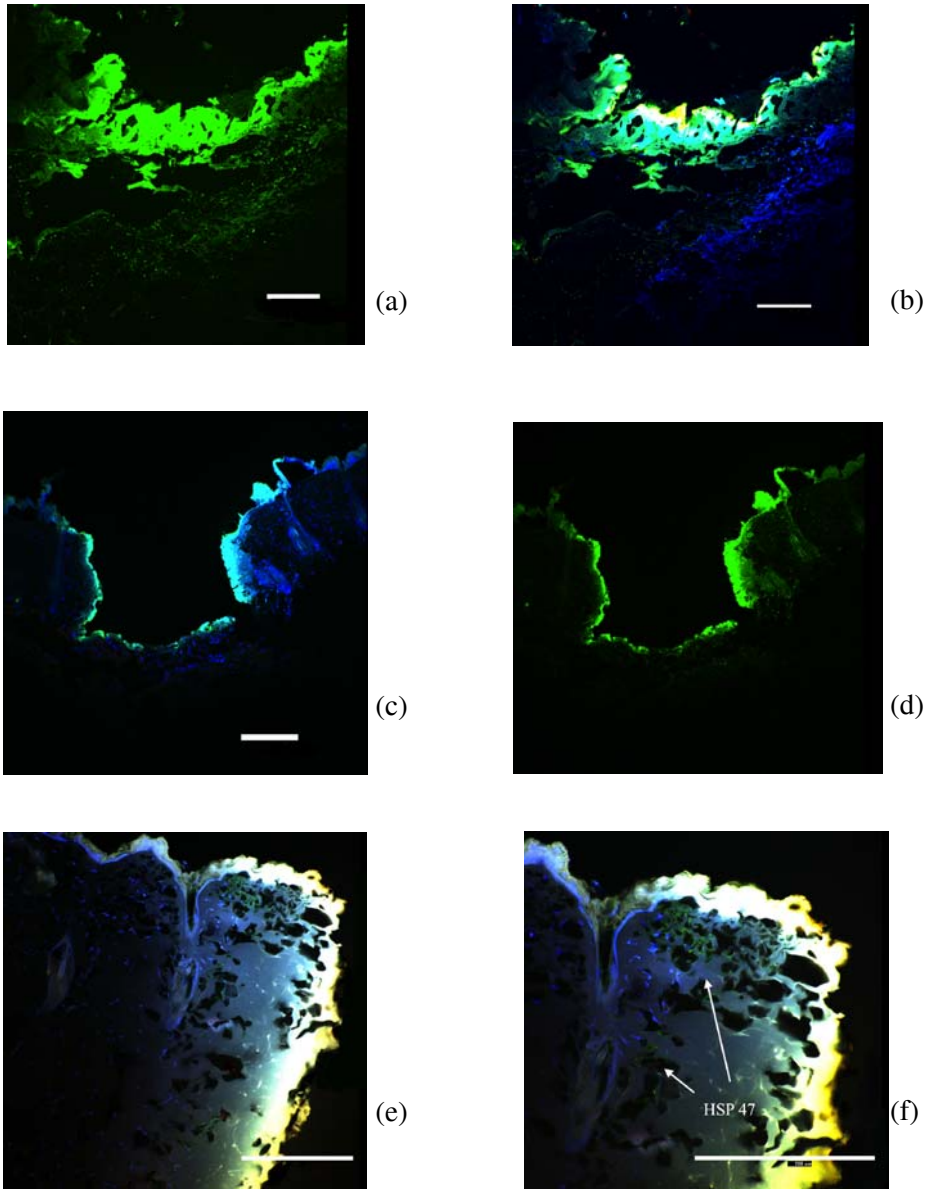


**FIG. 11:** Confocal microscopic visualization of immunolabeling 24 h after laser-induced ablation. Comparison of CW and short-pulse laser-induced damage. CW laser-induced damage (average power = 1.4 W, exposure time = 10 s). Multiple channel image (a) and green channel image of laser-induced lesion using CW laser (b). Short-pulse laser-induced damage (energy per pulse = 1.5 mJ, pulse width = 200 ns). Multiple channel image (c) and green channel image of laser-induced lesion using short-pulse laser (d); enlarged images of damage crater induced by short-pulse laser: 10× (e) and 20× (f). Green = HSP47 (scale bar = 200 μm) [reproduced from (Sajjadi et al., 2013)]

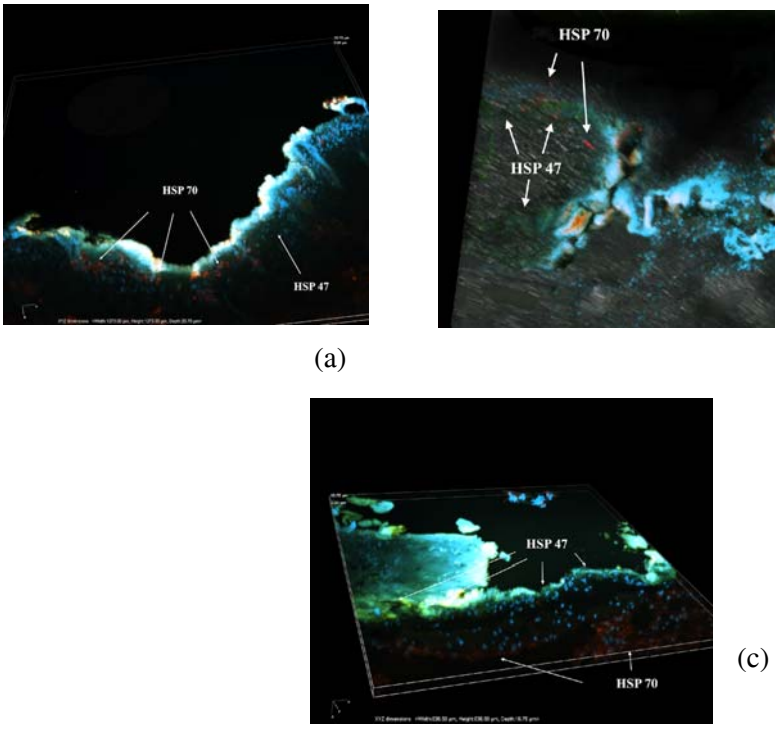


(a) (b)

(c)

**FIG. 12:** 3D Image of skin (thickness = 20 μm) lesion induced by short-pulse laser visualized with confocal microscope. Three-dimensional images of the cross section of tissue were reconstructed from the optical scans obtained for each sample image. Optical scans were obtained at 1-μm intervals through a 20-μm thick tissue section. Green and red arrows show the regions where HSP47 and 70 are expressed in the tissue. HSP70 and 47 are visualized at 2-h (a), 4-h (b), and 8-h (c) post-irradiation. Energy per pulse = 1.5 mJ, pulse width = 200 ns. Red = HSP70, green = HSP47, blue = DAPI [reproduced from (Sajjadi et al., 2013)]

### 5.4 Modeling of Plasma-Mediated Ablation

Due to the highly scattering feature of tissue, it is difficult to experimentally measure plasma formation inside turbid tissue. Instead semitransparent pure water was used because water is a primary content of biological tissues, occupying 60–70% of human body weight. Figure 14 compares the simulated plasma formations in water with the experimental observations for two different pulse energies 440 μJ and 3200 μJ, respectively. The laser pulse is 30 ps at a wavelength of 1064 nm with a constant focusing angle of $22^{o}$. The laser beam was converged to a focal spot 4.7 μm in diameter inside the distilled water. The experimental photos of the luminescent plasmas were taken with an open shutter in a dark room by

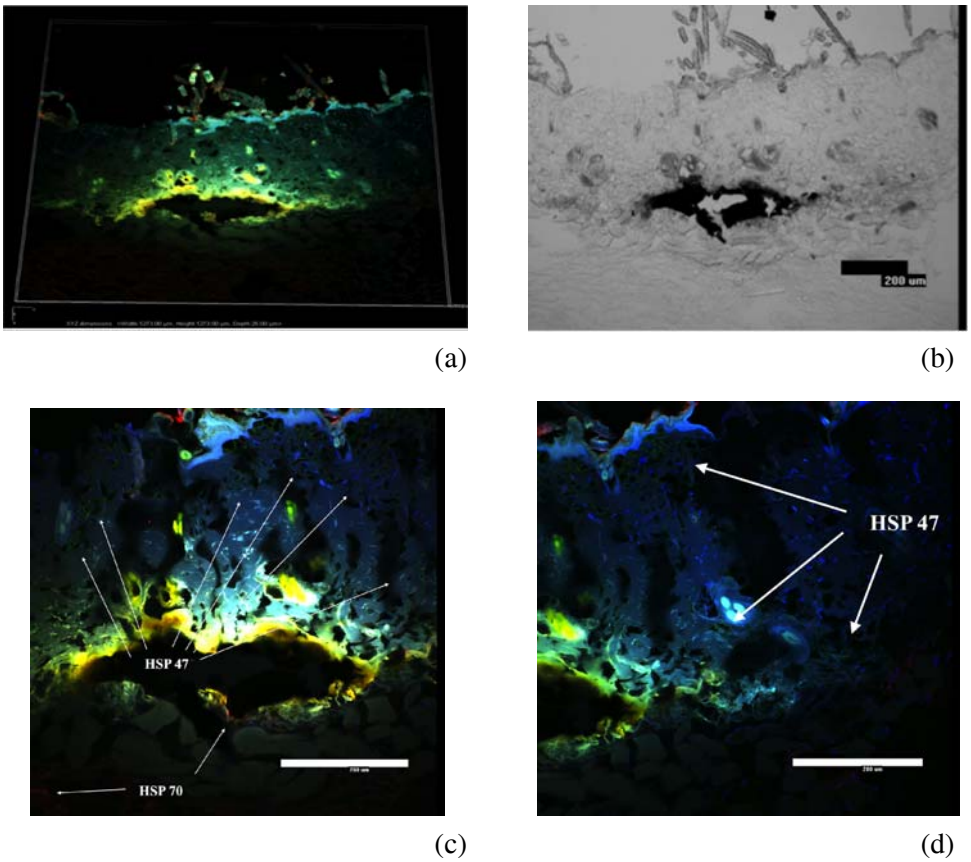


**FIG. 13:** Laser irradiated skin lesion (laser beam is focused underneath the skin) 24-h post-irradiation. Energy per pulse = 1.5 mJ, pulse width = 200 ns, green = HSP47, blue = DAPI. 3D image (a); visible light image (b); 2× multi-channel image of the lesion (c); 4× multi-channel image of the lesion (d). Green and red arrows show the regions where HSP47 and 70 are expressed in the tissue (scale bar = 200 μm) [reproduced from (Sajjadi et al., 2013)]

Vogel et al. (1996). The numerical pictures are obtained by calculating the time average of the accumulated free electrons during the breakdown period. As shown in the figure, the formed plasma clouds predicted by the numerical model match very well with the experimental measurements. It should be pointed out that the plasma luminescence photos taken in the experiment might not reflect the exact boundary of plasmas; while the critical plasma density value set in the simulation is also an assumption.

Figure 15 shows plasma formation in water with a 300-fs pulse at a wavelength of 580 nm. The laser has superthreshold pulse energy with a focusing angle of $16^{o}$. The focal spot size is 4.7 μm in diameter. In this case, ablation begins at $t_0$

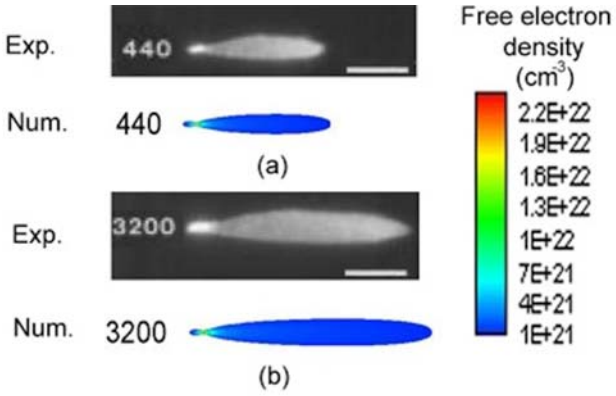


**FIG. 14:** Comparison of the formed plasma shapes between modeling and experimental photos in Vogel et al. (1996) for ablation in water with a 30-ps pulse at a wavelength of 1064 nm: a) plasma formed at a pulse energy of 440 μJ; b) plasma formed at a pulse energy of 3200 μJ. The laser is incident from the right. The bar represents a length of 100 μm [reproduced from (Jiao and Guo, 2011)]

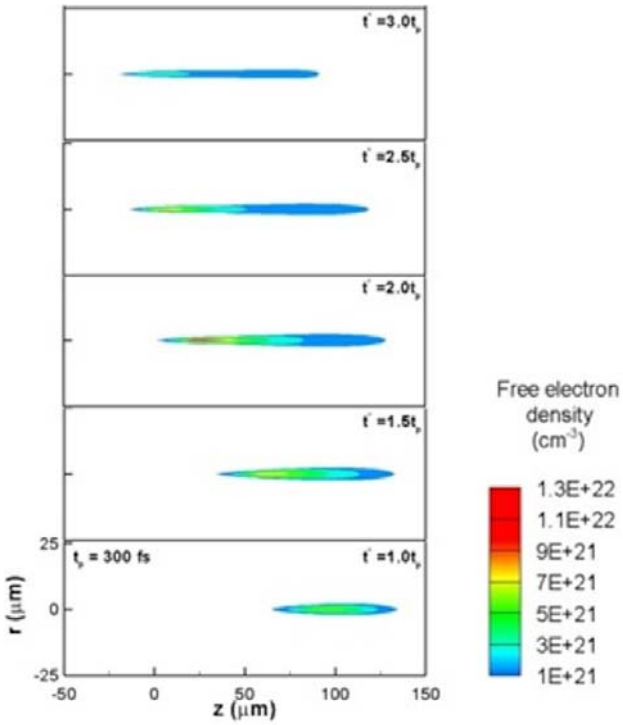


**FIG. 15:** Free electron distributions at various time instants in water induced by a 300-fs pulse ($\lambda$ = 580 nm, $\theta R = 16^o$, $\sigma_{ap}$ = 360 cm$^{-1}$. The light is incident from the right) [redrawn from (Jiao and Guo, 2011)]

= $0.6t_p$ in an upstream location, $z$ = 113 μm. This location is behind the pulse peak location ($z = 1.4ct_p$ = 95 μm) because of the delay existed between avalanche ionization and multiphoton ionization. It is very clear that the ablation front moves towards the focus and finally exceeds the focus at time instants $t^* = 2.5t_p$ and $t^* = 3.0t_p$. This is in contrast with the behavior of the 30-ps laser ablation where ablation front develops from the focus towards the incoming laser. It is also observed that the plasma cloud expands in the time period from $t^* = 0$ to $2.5t_p$, and then shrinks.

### 5.5 Crater Formation during the Plasma-Mediated Ablation

The ablation of material forms craters along the ablated pathway. Since soft tissue is deformable, it is not easy to determine its crater shape. To demonstrate crater formation, we used corundum as an example. The electron cooling time and lattice heating time for metals are reported as 1 ps and 100 ps, respectively (Nolte et al., 1997). For extremely short pulses, the pulse widths are much shorter than the electron cooling time and lattice heating time. The effects of electron–lattice coupling and heat diffusion could be negligible during the short pulse duration. Consequently, the local absorbed laser irradiance could be determined as

$$\Delta E_l(r, z) = \int_0^{t_d} \nabla \cdot q_{rad}(r, z, t)dt \tag{11}$$

In the calculation of the crater shape, the materials were assumed ablated only after they absorbed enough laser energy to evaporate. The minimum energy required to evaporate the material is estimated as

$$\Delta E_e = C_p(T_m - T_0) + \Delta H_m + C_p(T_v - T_m) + \Delta H_v \ , \tag{12}$$

where $C_p$ is the specific heat. The room temperature $T_0$ = 298 K is the initial temperature of the material; $T_m$ and $T_v$ are the melting and boiling points, respectively; $\Delta H_m$ and $\Delta H_v$ are the latent heat of melting and vaporization, respectively. Significant evaporation occurs when $\Delta E_l(r, z)$ becomes larger than $\Delta E_e$.

Figure 16 plots the crater profile ablated by laser fluence $F$ = 5.5 J/cm$^2$ at λ = 800 nm in corundum (Jiao, 2011). The solid line represents the experimentally measured crater profile by Guizard et al. (2002). The dashed line stands for the crater profile predicted by the numerical model. Since the pulse width, $t_p$ = 58 fs, is much shorter than the lattice heating time (~100 ps), the accumulated laser energy stored in the plasma is directly transferred to lattice without thermal diffusion. The rapid temperature rise in the lattice leads to the occurrence of evaporation. The onset of evaporation occurring is determined by Eq. (12). As illustrated in the figure, the crater shape predicted by the numerical model generally match very well with the experimental measurement in the literature. The deviation between the experimental measurement and numerical predictions on the corundum surface may be due to: firstly, the impurities existing on the corundum surface may facilitate

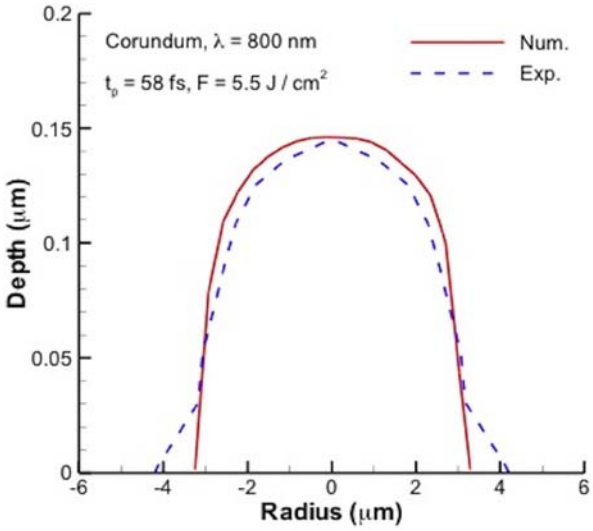


**FIG. 16:** Crater profile ablated in corundum by a pulse of $t_p$ = 58 fs at $F$ = 5.5 J/cm$^2$ at λ = 800 nm and comparison with the experimental results of (Jiao, 2011) [reproduced from (Jiao, 2011)]

the generation of the initial electrons and thus largely reduce the ablation threshold. Secondly, the plasma-mediated ablation is always associated with mechanical effects, e.g., shock wave generation.

## 6. CONCLUSIONS

In this manuscript, a review of common existing thermal analysis techniques is presented. A minimally invasive technique for ablating subsurface tumors through the use of a converging beam from an ultrashort pulsed laser focused at the tumor location is presented. Studying the characteristics of ablated region is presented using histological, immunohistochemical, and mathematical techniques. It is shown that focusing the beam from an ultrashort pulse laser directly at the tumor site results in precise, clean ablation without significantly affecting the surrounding epidermal and dermal layers.

Analysis of the distribution and time course of appearance of heat shock proteins provides a valuable means to understand the spatial and temporal effects of laser irradiation on tissue processes of tissue destruction and healing. The results presented here indicate that following laser irradiation of mouse skin, HSP70 defines biochemically the thermal damage zone in which cells are targeted for destruction, and HSP47 indicates a zone of sublethal thermal stress and may define the time course of wound healing. Finally, the expression of HSPs, particularly HSP47, on all sides of subsurface lesions produced with a focused-beam laser provide new evidence that focused lasers can produce precise subsurface lesions.

## REFERENCES

Aksan, A., McGrath, J., and Nielubowicz, Jr., D. S., Thermal damage prediction for collagenous tissues. Part I: A clinically relevant numerical simulation incorporating heating rate dependent denaturation, *J. Biomech. Eng.*, vol. 127, pp. 85–97, 2005.

Allemann, I. B. and Kaufman, J., Fractional photothermolysis — an update, *Lasers Med. Sci.*, vol. 25, pp. 137–144, 2010.

Anderson, R. R. and Parrish, J. A., Selective photothermolysis: precise microsurgery by selective absorption of pulsed radiation, *Science*, vol. 220, pp. 524–527, 1983.

Anderson, R. R., Dermatological history of the ruby laser: the long story of short pulses, *Arch. Dermatol.*, vol. 139, pp. 70–74, 2003.

Armstrong, W. B., Neev, J. A., Da Silva, L. B., Rubenchik, A. M., and Stuart, B. C., Ultrashort pulse laser ossicular ablation and stapedotomy in cadaveric bone, *Lasers Surg. Med.*, vol. 30, pp. 216–220, 2002.

Arora, D., Skliar, M., and Roemer, R. B., Minimum-time thermal dose control of thermal therapies, *IEEE Trans. Biomed. Eng.,* vol. 52, pp. 191–200, 2005.

Bass, L. S. andTreat, M. R., Laser tissue welding: a comprehensive review of current and future applications, *Lasers Surg. Med.*, vol. 17, pp. 315–349, 1995.

Bille, J. F., Harner, C. F. H., and Loesel, F., *New Frontiers in Vision and Aberration-Free Refractive Surgery*, Heidelberg, Germany: Springer Press, 2002.

Boehm, K., Saunders, A., Werner, J., and Lis, J. T., Transcription factor and polymerase recruitment, modification, and movement on hsp70 *in vivo* in the minutes following heat shock, *Molec. Cell. Biol.*, vol. 23, pp. 7628–7637, 2003.

Boppart, S. A., Herrmann, J., Pitris, C., Stamper, D. L., Brezinski, M. E., and Fujimoto, J. G., High-resolution optical coherence tomography-guided laser ablation of surgical tissue, *J. Surg. Res.*, vol. 82, pp. 275–284, 1999.

Brown, S. A., Farkas, J. P., Arnold, C., Hatef, D. A., Kim, J., Hoopman, J., and Kenkel, J. M., Heat shock proteins 47 and 70 expression in rodent skin model as a function of contact cooling temperature: Are we overcooling our target?, *Lasers Surg. Med.*, vol. 39, pp. 504–512, 2007.

Bukau, B., Weissman, J., and Horwich, A., Molecular chaperones and protein quality control, *Cell*, vol. 125, pp. 443–451, 2006.

Chen, B., Thomsen, S. L., Thomas, R. J., and Welsh, A. J., Modeling thermal damage in skin from 2000-nm laser irradiation, *J. Biomed. Opt.*, vol. 11, no. 6, p. 0.64028, 2006.

Chen, W. R., Lu, H., and Nordquist, R. E., Mechanism of laser immunotherapy — role of immunoadjuvant and selective photothermal laser–tissue interaction, *Proc. SPIE 2002*, vol. 4536, pp. 82–89, 2002.

Chen, W. R., Phillips, C. S., Adams, R. L., Bartels, K. E., and Nordquist, R. E., Indocyanine green in-situ administration and photothermal destruction of tumor tissue using an 808-nm diode laser, *Proc. SPIE 1996*, vol. 2681, pp. 94–101, 1996.

Chung, S. H. and Mazur, E., Femtosecond laser ablation of neurons in C elegans for behavioral studies, *Appl. Phys. A*, vol. 96, pp. 335–341, 2009.

Dafforn, T. R., Della, M., and Miller, A. D., The molecular interactions of heat shock protein 47 (Hsp47) and their implications for collagen biosynthesis, *J. Biolog. Chem.*, vol. 276, no. 52, pp. 49310–49319, 2001.

Dai, T., Diagaradiane, P., Yaseen, M. A., Pikkula, B. M., Thomsen, S., and Anvari, B., Laser induced thermal injury to dermal blood vessels: Analysis of wavelength (585 nm vs 595 nm), cryogen spray cooling and wound healing effects, *Lasers Surg. Med*., vol. 37, pp. 210–218, 2005.

Dams, S. D., de Liefde-van Beest M., Nuijs, A. M., Oomens, C. W. J., and Baaijens, F. P. T., Pulsed heat shocks enhance procollagen type I and procollagen type III expression in human dermal fibroblasts, *Skin Res. Technol*., vol. 16, pp. 354–364, 2010.

Davidson, S. R. H., Vitkin, I. A., Sherar, M. D., and Whelan, W. M., Characterization of measurement artifacts in fluoroptics temperature sensors: Implications of laser thermal therapy at 810 nm, *Lasers Surg. Med.*, vol. 36, pp. 297–306, 2005.

Dayan, A., Goren, A., and Gannot, I., Theoretical and experimental investigation of the thermal effects within body cavities during transendoscopical $CO_2$ laser based surgery, *Lasers Surg. Med*., vol. 35, pp. 18–27, 2004.

Dewhirst, M. W., Vigianti, B. L., Lora-Michiels, M., Hoopes, P. J., and Hanson, M., Thermal dose requirement for tissue effect: Experimental and clinical Findings, *Proc. SPIE 2003*, vol. 4954, pp. 37–57, 2003.

Diaz, S. H., Lavernia, E. J., and Wong, B. J. F., Modeling the thermal response of porcine cartilage during laser irradiation, *IEEE J. Select. Topics Quant.Electron*., vol. 7, pp. 944–951, 2001.

Docchio, F., Lifetimes of plasmas induced in liquids and ocular media by single Nd-Yag laser-pulses of different duration, *Europhys. Lett*., vol. 6, pp. 407–412, 1988.

Fahey, M., Mitra, K., Onyejekwe, O., and Mason, H. L., Precise dental ablation using ultrashort pulsed 1552 nm laser, *Int. J. Heat Mass Transfer*, vol. 51, pp. 5732–5739, 2008.

Fischer, J. P., Dams. J., Gotz, M. H., Kerker, E., Loesel, F. H., Messer, C., Suhm, M. H., and Bille, J. F., Plasma-mediated ablation of brain tissue with picosecond laser pulses, *Appl. Phys. B*, vol. 58, pp. 493–499, 1994.

Fischer, J. P., Juhasz, T., and Bille, J. F., Time resolved imaging of the surface ablation of soft tissue with IR picosecond laser pulses, *Appl. Phys. A*, vol. 64, pp. 181–189, 1997.

Fried, N. M. and Walsh, J. R., Dye-assisted laser skin closure with pulsed radiation: An in vitro study of weld strength and thermal damage, *J. Biomed. Opt*., vol. 3, pp. 401–408, 1998.

Georgala, D. L. and Boothroyd, M., A rapid immunofluorescence technique for detecting salmonellae in raw meat, *J. Hygiene*, vol. 62, pp. 319–327, 1964.

Gomer, C. J., Rucker, N., Ferrario, A., and Wong, S., Properties and applications of photodynamic therapy, *Radiation Res*., vol. 120, pp. 1–18, 1989.

Gratzl, T., Dohr, G., Schmidt-Kloiber, and H., Reichel, E., Histological distinction of mechanical and thermal defects produced by nanosecond laser pulses in striated muscle at 1064 nm, *Proc. SPIE 1991*, vol. 1427, pp. 55–62, 1991.

Guizard, S., Semerok, A., Gaudin, J., Hashida, A., Martin, P., and Quere, F., Femtosecond laser ablation of transparent dielectrics: measurement and modelisation of crater profiles, *Appl. Surface Sci.*, vol. 186, pp. 364–368, 2002

Guo, Z. and Hunter, B., Advances of ultrafast radiative transfer modeling and applications: a review, *Heat Transfer Research*, vol. 44, nos. 3–4, pp. ....., 2013.

Hahn, G. M., Potential for therapy of drugs and hyperthermia, *Cancer Res*., vol. 39, pp. 2264–2268, 1979.

Han, M., Giese, G., Zickler, L., Sun, H., and Bille, J., Mini-invasive corneal surgery and imaging with femtosecond lasers, *Optics Express 2004*, vol. 12, pp. 4275–4281, 2004.

Hawes, C. R. and Satiat-Jeunemaitre, B., *Plant Cell Biology*, Oxford University Press, 2001.

Heisterkamp, A., Mamom, T., Drommer, W., Ertmer, W., and Lubatschowski, H., Photodisruption with ultrashort laser pulses for intrastromal refractive surgery, *Laser Phys*., vol. 13, pp. 743–748, 2003.

Helbig, D., Moebius, A., Simon, J. C., and Paasch, U., Nonablative skin rejuvenation devices and the role of heat shock protein 70: results of a human skin explant model, *J. Biomed. Opt*., vol. 15, no. 3, p. 038002, 2010.

Huang, H. and Guo, Z., Ultrashort pulsed laser ablation and stripping of freeze-dried dermis, *Lasers Med. Sci*., vol. 25, no. 4, pp. 517–524, 2010.

Huang, H. and Guo, Z., Human dermis separation via ultrashort pulsed laser plasma-mediated ablation, *J. Phys. D: Appl. Phys.*, vol. 42, 165204 (9 p.), 2009.

Hunter, B. and Guo, Z., Conservation of asymmetry factor in phase function discretization for radiative transfer analysis in anisotropic scattering media, *Int. J. Heat Mass Transfer*, vol. 55, pp. 1544–1552, 2012a.

Hunter, B. and Guo, Z., Phase-function normalization for accurate analysis of ultrafast collimated radiative transfer, *Appl. Opt*., vol. 51, pp. 2192–2201, 2012b.

Jacques, S. L., How tissue optics affect dosimetry for photochemical, photothermal, and photomechanical mechanisms of laser–tissue interaction, *Proc. SPIE 1991*, vol. 1599, pp. 316–322, 1991.

Jacques, S. L., Laser–tissue interactions, *Surg. Clin. North Am*., vol. 72, no. 3, pp. 531–58, 1992.

Jeong, S. W., Liu, H., and Chen, W. R., Temperature control in deep tumor treatment, *Proc. SPIE 5968*, *Saratov Fall Meeting 2002: Optical Technologies in Biophysics and Nedicine IV*, October 14, 2003, pp. 210–216, 2003.

Jiao, J. and Guo, Z., Analysis of plasma-mediated ablation in aqueous tissue, *Appl. Surface Sci.*, vol. 258, pp. 6266–6271, 2012.

Jiao, J. and Guo, Z., Modeling of ultrashort pulsed laser ablation in water and biological tissues in cylindrical coordinates, *Appl. Phys. B*, vol. 103, pp. 195–205, 2011.

Jiao, J. and Guo, Z., Thermal interaction of short-pulsed laser focused beams with skin tissues, *Phys. Med. Biol*., vol. 54, pp. 4225–4241, 2009.

Jiao, J., *Simulation of Laser–tissue Thermal Interaction and Plasma-Mediated Ablation*, Ph.D. Dissertation, Rutgers University, 2011.

Kennedy, P. K., A first-order model for computation of laser-induced breakdown thresholds in ocular and aqueous-media. I. Theory, *IEEE J. Quant. Electron*., vol. 31, pp. 2241–2249, 1995.

Kennedy, P. K., Boppart, S. A., Hammer, D. X., Rockwell, B. A., Noojin, G. D., and Roach, W. P., A first-order model for computation of laser-induced breakdown thresholds in ocular and aqueous-media. II. Comparison to experiment, *IEEE J. Quant. Electron*., vol. 31, pp. 2250–2257, 1995.

Khan, M. H., Sink, R. K., Manstein, D., Eimerl, D., and Anderson, R. R., Intradermally focused infrared laser pulses: Thermal effects at defined tissue depths, *Lasers Surg. Med*., vol. 36, pp. 270–280, 2005.

Kim, B. M., Feit, M. D., Rubenchik, A. M., Joslin, E. J., Celliers, P. M., Eichler, J., and Da Silva, L. B., Influence of pulse duration on ultrashort laser pulse ablation of biological tissues, *J. Biomed. Opt*., vol. 6, pp. 332–338, 2001.

Kim, K. and Guo, Z., Ultrafast radiation heat transfer in laser tissue welding and soldering, *Numer. Heat Transfer A*, vol. 46, pp. 23–40, 2004.

Kimel, S., Svaasand, L. O., Kelly, K. M., and Nelson, J. S., Synergistic photodynamic and photothermal treatment of port-wine stain, *Lasers Surg. Med*., vol. 34, pp. 80–82, 2004.

Koenig, K., Wang, B., Riemann, I., and Kobow, J., Cornea surgery with nanojoule femtosecond laser pulses, *Proc. SPIE 2005*, vol. 5688, pp. 288–293, 2005.

Kurtz, R. M., Elner, V., Liu, X., and Juhasz, T., Plasma-mediated ablation of biological tissue with picosecond and femtosecond laser pulses, *Proc. SPIE 1997*, vol. 2975, pp. 192–200, 1997.

Laubach, H. J., Tannous, Z., Anderson, R. R., and Manstein, D., Skin response to fractional photothermolysis, *Lasers Surg. Med.*, vol. 38, pp. 142–149, 2006.

Leger, J. P., Smith, F. M., and Currie, R. W., Confocal microscopic localization of constitutive and heat shock–induced proteins HSP70 and HSP27 in the rat heart, *Circulation*, vol. 102, pp. 1703–1709, 2000.

Loesel, F. H., Fischer, J. P., Götz, M. H., Horvath, C., Juhasz, T., Noack, F., Suhm, N., and Bille, J. F., Non-thermal ablation of neural tissue with femtosecond laser pulses, *Appl. Phys.*, vol. 66, pp. 121–128, 1998.

Loesel, F. H., Niemez, M. H., Bille, J. F., and Juhasz, T., Laser-induced optical breakdown on hard and soft tissues and its dependence on the pulse duration: Experiment and model, *IEEE J. Quant. Electron.*, vol. 32, pp. 1717–1722, 1996.

Majaron, B., Srinivas, S. M., Huang, H. L., and Nelson, J. S., Deep coagulation of dermal collagen with repetitive Er:YAG laser irradiation, *Lasers Surg. Med.*, vol. 26, pp. 215–222, 2000.

Manns, F., Milne, P. J., Gonzalez-Cirre, X., Denham, D. B., Parel, J. M., and Robinson, D. S., *In situ* temperature measurements with thermocouple probes during laser interstitial thermometry (LITT): quantification and correction of a measurement artifact, *Lasers Surg. Med.*, 23, pp. 94–103, 1998.

Manstein, D., Herron, G. S., Sink, R. K., Tanner, H., and Anderson, R. R., Fractional photothermolysis: A new concept for cutaneous remodeling using microscopic patterns of thermal injury, *Lasers Surg. Med.*, vol. 34, pp. 426–438, 2004.

Mark, M. G., Eichler, K., Straub, R., Lehnert, T., and Vogl, T. J., MR-guided laser-induced thermotherapy of head and neck tumors, *Med. Laser Appl.*, vol. 19, pp. 91–97, 2004.

McKenzie, A. L., Physics of thermal process in laser–tissue interaction, *J. Phys. Med. Biol.*, vol. 35, pp. 1175–1209, 1990.

Milne, P. J., Parel, J. M., Manns, F., Cirre, X. G., and Robinson, D. S., Development of stereotactically guided laser interstitial thermotherapy of breast cancer: in situ measurement and analysis of the temperature field in ex vivo and in vivo adipose tissue, *Lasers Surg. Med.*, vol. 26, pp. 67–75, 2000.

Mito, K., A needle type therapeutic system incorporating laser light and lumen for immunotherapy of cancer growing in deep organs, *J. Med. Eng. Technol.*, vol. 30, pp 121–126, 1996.

Neev, J., Carrasco, W. A., Armstrong, W. B., Da Silva, L. B., Feit, M. D., Matthews, D. L., Perry, M. D., Rubenchik, A. M., and Stuart, B. C., Applications of ultrashort pulse lasers for hard tissue surgery, *Proc. SPIE 1996*, vol. 2671, pp. 149–157, 1996.

Niemz, M. H., Klancnik, E. G., and Bille, J. F., Plasma-mediated ablation of corneal tissue at 1053 nm using a Nd:YLF oscillator/regenerative amplifier laser, *Lasers Surg. Med.*, vol. 11, pp. 426–431, 1991.

Niemz, M. H., *Laser–Tissue Interactions*, Berlin: Springer-Verlag, 1996.

Niemz, M. H., *Laser–Tissue Interactions: Fundamentals and Applications*, 3rd ed., Heidelberg, Germany: Springer Press, 2003.

Noack, J. and Vogel, A., Laser-induced plasma formation in water at nanosecond to femtosecond time scales: Calculation of thresholds, absorption coefficients, and energy density, *IEEE J. Quant. Electron.*, vol. 35, pp. 1156–1167, 1999.

Nolte, S., Momma, C., Jacobs, H., Tunnermann, A., Chichkov, B. N., Wellegehausen, B., and Welling, H., Ablation of metals by ultrashort laser pulses, *J. Opt. Soc. Am. B, Opt. Phys*., vol. 14, pp. 2716–2722, 1997.

Nordquist, R. E., Nordquist, J. A., Agee, J. C., Blomquist, C. M., and Chen, W. R., Morphological studies of metastatic mammary rat tumors after laser immunotherapy treatment, *Proc. SPIE 1998*, vol. 3254, pp. 36–40, 1998.

O'Connell-Rodwell, C. E., Mackanos, M. A., Simanovskii, D., Cao, Y. A., Bachmann, M. H., Schwettman, H. A., and Contag, C. H., *In vivo* analysis of heat-shock-protein-70 induction following pulsed laser irradiation in a transgenic reporter mouse, *J. Biomed. Opt*., vol. 13, no. 3, p. 030501-3, 2008.

O'Neal, D. P., Hirsch, L. R., Halas, N. J., Payne, J. D., and West, J. L., Photo-thermal tumor ablation in mice using near infrared-absorbing nanoparticles, *Cancer Lett*., vol. 209, pp. 171–176, 2004.

Onyejekwe, O., Sajjadi, A. Y., Abdulla, U., Mitra, K., and Grace, M. S., Mathematical models for analyzing tissue ablation performed using short-pulse laser, *Proc. ASME*, vol. 11626, pp. 179–185, 2009.

Oraevsky, A. A., Da Silva, L. B., Rubenchik, A. M., Feit, M. D., Glinsky, M. E., Perry, M. D., Mammini, B. M., Small, W. I. V., and Stuart, B. C., Plasma mediated ablation of biological tissues with nanosecond-to-femtosecond laser pulses: Relative role of linear and nonlinear absorption, *IEEE J. Select. Topics Quant. Electron.*, vol. 2, pp. 801–809, 1996.

Ozturk, S., Hoopman, J., Brown, S. A., Nojima, K., Saboorian, H., Acikel, C., and Kenkel, J., A useful algorithm for determining fluence and pulse width for vascular targets using 1064 nm Nd:YAG laser in animal model, *Lasers Surg. Med*., vol. 34, pp. 420–425, 2004.

Pal, G., Sajjadi, A. Y., Mitra, K., and Grace, M. S., Transient radiation modeling of short-pulse laser detection of tumors in animal model, *Proc. IEEE Signal Process. Soc.*, *Conference record of the 43 Asilomar Conf. on Signals, Systems, and Computers*, New York: IEEE Press Books, pp. 1609–1613, 2009.

Panjehpour, M., Wilke, A., Frazier, D. L., and Overholt, B.F., Hyperthermia treatment using a computer controlled Nd:YAG laser system in combination with surface cooling, *Proc. SPIE 1991*, vol. 1427, pp. 307–315, 1991.

Pech, M., Wieners, G., Fischbach, F., Hengst, S., Beck, A., Warschewske, G., Hanninen, E. L., Wust, P., and Ricke, J., Synchronous CT-guided brachytherapy in patients at risk for incomplete interstitial laser ablation of liver malignancies, *Med. Laser Appl*., vol. 19, pp. 73–82, 2004.

Pennes, H. H., Analysis of tissue and arterial blood temperatures in the resting forearm, *J. Appl. Physiol*., vol. 1, pp. 93–122, 1984.

Prahl, S. A., Pearson, S. D., and Jacques, S. L., Rate process models for thermal welding, *Laser–Tissue Interaction VIII Proc. SPIE*, vol. 2975, pp. 245–252, 1997.

Presnell, J. K. and Schreibman, M. P., *Animal Tissue Techniques*, Baltimore and London: The John Hopkins University Press, 1997.

Raskin, B. and Fany, R. R., Laser treatment for neovascular formation, *Lasers Surg. Med*., vol. 34, pp. 189–192, 2004.

Rink, K., Delacretaz, G., and Salathe, R. P., Fragmentation therapy of current laser lithotripters, *Lasers Surg. Med*., vol. 16, pp. 134–146, 1995.

Robinson, D. S., Parel, J. M., Denham, D. B., Gonzalez-Cirre, X., Manns, F., Milne, P. J., Schachner, R. D., Herron, A. J., Comander, J., and Hauptmann, G., Interstitial laser hyperthermia model

development for minimally invasive therapy of breast carcinoma, *J. Am. Coll. Surg*., vol. 186, pp. 284–292, 1998.

Rome, C., Couillaud, F., and Moonen, C. T. W., Spatial and temporal control of expression of therapeutic genes using heat shock protein promoters, *Methods*, vol. 35, pp. 188–198, 2005.

Sacks, Z. S., Kurtz, R. M., Juhasz, T., and Mourou, G., Femtosecond subsurface photodisruption in scattering human tissues using long infrared wavelengths, *Proc. SPIE 2001*, vol. 4241, pp. 98–111, 2001.

Sajjadi, A. Y., Mitra, K., and Grace, M. S., Ablation of subsurface tumors using an ultrashort pulse laser, *Opt. Lasers Eng*., vol. 49, no. 3, pp. 451–456, 2011a.

Sajjadi, A. Y., Mitra, K., and Grace, M. S., Analysis of short pulse laser interaction with tissues for tumor detection, *Proc. ASME*, vol. 11945, pp. 293–300, 2009.

Sajjadi, A. Y., Mitra, K., and Grace, M. S., Expression of heat shock proteins 70 and 47 in tissues following short-pulse laser irradiation: assessment of thermal damage and healing, *Med. Eng. Phys*., 2013a (in press).

Sajjadi, A. Y., Mitra, K., and Grace, M. S., Short-pulse laser-based system for detection of tumors: administration of gold nanoparticles enhances contrast, *J. Nanotechnol. Eng. Med.*, vol. 3, no. 2, p. 021002, 2012.

Sajjadi, A. Y., Mitra, K., and Grace, M. S., Visualization of heat shock proteins for quantifying laser-induced thermal ablation of biological tissues, *Proc. ASME 2010*, vol. 53483, pp. 997–999, 2010.

Sajjadi, A. Y., Onyejekwe, O., Raje, S., and Mitra, K., Thermal ablation of mouse skin tissue using ultrashort pulse 1550 nm laser, *Proc. ASME 2008*, vol. 56396, pp. 347–353, 2008a.

Sajjadi, A. Y., Pal, G., Mitra, K., and Grace, M. S., Using gold nanoparticles to enhance the contrast in optical imaging using short-pulse laser, *Proc. Biomed. Opt. (BIOMED)*, p. BTu3A.10, 2011c.

Sajjadi, A. Y., Raje, S., Mitra, K., and Grace, M. S., Ablation of tumors using an ultrashort-pulse laser, *Proc. ASME 2008*, p. 192415, 2008b.

Sajjadi, A. Y., *Ultrashort Pulse Laser–Tissue Interaction for Ablation and Diagnostics of Subcutaneous Tumors*, Ph.D. Thesis, Florida Institute of Technology, 2012**[Q1]**.

Sajjadi, A., Onyejekwe, O., Raje, S., Mitra, K., and Grace, M., Thermal ablation of mouse skin tissue using ultra short pulse 1552 nm laser, *Proc. Int. ASME Conf.*, vol. 56396, pp. 347–353, 2008c.

Sherratt, J. A. and Murray, J. D., Epidermal wound healing: a theoretical approach, *Comments Theor. Biol*., vol. 2, pp. 315–333, 1992.

Snoeckx, L. H. E. H., Cornelussen, R. N., Van Neiuwenhoven, F. A., Reneman, R. S., and Van der Vusse, G. J., Heat shock proteins and cardiovascular pathophysiology, *Physiol. Rev*., vol. 81, pp. 1461–1497, 2002.

Steel, G. J., Fullerton, D. M., Tyson, J. R., and Stirling, C. J., Coordinated activation of hsp70 chaperones, *Science*, vol. 303, pp. 98–101, 2004.

Steiner, R., Interactions of laser radiation with biological tissue, in: H. Berlien and G. Müller (Eds.), *Applied Laser Medicine*, Berlin–Heidelberg–New York: Springer, pp. 101–106, 2003.

Sun, M. H., Wickersheim, K. A., and Kim, J., Fiber optic temperature sensors in the medical setting, *Optical Fibers in Medicine IV*, *Proc. SPIE 1989*, vol. 1067, pp. 15–20, 1989.

Sun, Q., Jiang, H., Liu, Y., Wu, Z., Yang, H., and Gong, Q., Measurement of the collision time of dense electronic plasma induced by a femtosecond laser in fused silica, *Opt. Lett*., vol. 30, pp. 320–322, 2005.

Tanehill, J. C., Anderson, D. A., and Pletcher, R. H., *Computational Fluid Mechanics and Heat Transfer*, 2nd ed., Washington DC: Taylor and Francis, 1984.

Thongsima, S., Zurakowski, D., and Manstein, D., Histological comparison of two different fractional photothermolysis devices operating at 1550 nm, *Lasers Surg. Med*., vol. 42, pp. 32–37, 2010.

Torres, J. H., Nelson, J. S., Tanenbaum, B. S., Milner, T. E., Goodman, D. M., and Anvari, B., Estimation of internal skin temperatures in response to cryogenic spray cooling implications for laser therapy of port wine stains, *IEEE J. Select. Topics Quant. Electron*., vol. 5, pp. 1058–1066, 1999.

Verena, K., Frank, F., and Ewa, R., Principles of lasers and biophotonic effects, *Photomed. Laser Surg*., vol. 22, pp. 411–417, 2004.

Verrico, A. K., Haylett, A. K., and Moore, J. V., *In vivo* expression of the collagen-related heat shock protein HSP47, following hyperthermia or photodynamic therapy, *Lasers Med. Sci.*, vol. 16, no. 3, pp. 192–198, 2001.

Vogel, A. and Venugopalan, V., Mechanisms of pulsed laser ablation of biology tissues, *Chem. Rev*., vol. 103, pp. 577–644, 2003.

Vogel, A., Nahen. K., Theisen, D., and Noack, J., Plasma formation in water by picosecond and nanosecond Nd:YAC laser pulses. II. Optical breakdown at threshold and superthreshold irradiance, *IEEE J. Select. Topics Quant. Electron.*, vol. 2, pp. 847–860, 1996.

Vogel, A., Noack, J., Huttman, G., and Paltauf, G., Mechanisms of femtosecond laser nanosurgery of cells and tissues, *Appl. Phys. B, Lasers Optics*, vol. 81, pp. 1015–1047, 2005.

Vogel, A., Noack, J., Nahen, K., Theisen, D., Birngruber, R., Hammer, D. X., Noojin, G. D., and Rockwell, B. A., Laser-induced breakdown in the eye at pulse duration from 80 ns to 100 fs, *Proc. SPIE 1998*, vol. 3255, pp. 34–49, 1998.

Waldow, S. M., Morrison, P. R., and Grossweiner, L. I., Nd:YAG laser-induced hyperthermia in a mouse tumor model, *Lasers Surg. Med*., vol. 8, pp. 510–514, 1988.

Wang, S., Diller, K. R., and Aggarwal, S. J., Kinetics study of endogenous heat shock protein 70 expression, *J. Biomech. Eng*., vol. 125, pp. 794–797, 2003.

Wang, S., Xie, W., Rylander, M. N., Tucker, P. W., Aggarwal, S., and Diller, K. R., HSP70 kinetics study by continuous observation of HSP-GFP fusion protein expression on a perfusion heating stage, *Biotechnol. Bioeng*., vol. 99, no. 1, pp. 146–154, 2008.

Wang, X. L. and Guo, Z., Effective removal of adhering cells via ultrashort laser pulses, *Opt. Laser Technol*., vol. 42, no. 2, pp. 447–451, 2010.

Waynant, W., *Lasers in Medicine*, Boca Raton, Florida: CRC Press LLC, 2002.

Welch, A. J., *Model of Thermal Injury Based on Temperature Rise in Fundus Exposed to Laser Radiation*, Brooks Air Force Base, TX: USFA School of Aerospace Medicine, 1975.

Welch, A. J., The thermal response of laser irradiated tissue, *IEEE J. Quant. Electron*., vol. 20, pp. 1471–1481, 1984.

Wells, P. B., Thomsen, S., Jones, M. A., Baek, S., and Humphrey, J. D., Histological evidence for the role of mechanical stress in modulating thermal denaturation of collagen, *Biomech. Model. Mechanobiol.*, vol. 4, pp. 201–210, 2005.

Welsh, A. J. and Van Gemert, M. J. C., *Optical-Thermal Response of Laser-Irradiated Tissue*, Heidelberg, Germany: Springer Press, 1995.

Wilkens, V., Wiemann, C., Koch, C., and Foth, H. J., Fiber-optic dielectric multilayer temperature sensor: in situ measurement in vitreous during Er:YAG laser irradiation, *Opt. Laser Technol*., vol. 31, pp. 593–599, 1999.

Wilmink, G. J., Opalenik, S. R., Haselton, F. R., Mackanos, M., Nanney, L., Contag, C. H., Davidson, J. M., and Jansen, E. D., *In vivo* optical imaging of hsp70 expression to assess collateral tissue damage associated with infrared laser ablation of skin, *J. Biomed. Opt*., vol. 13, no. 5, pp. 054066/1–12, 2008.

Xie, H., Buckley, L., Pralh, S., Shaffer, B., and Gregory, K., Thermal damage control of dye-assisted laser tissue welding: effects of dye concentration, *SPIE Proc. Lasers Surgery 2001*, vol. 4244, pp. 189–192, 2001.

Yamasaki, A., Tamamura, K., Sakurai, Y., Okuyama, N., Yusa, J., and Ito, H., Remodeling of the rat gingiva induced by $CO_2$ laser coagulation mode, *Lasers Surg. Med*., vol. 40, pp. 695–703, 2008.

Youn, J. I., Sweet, P., Peavy, G. M., and Venugopalan, V., Mid-IR laser ablation of articular and fibro-cartilage: a wavelength dependence study of thermal injury and crater morphology, *Lasers Surg. Med.*, vol. 38, pp. 218–228, 2006.

Zhou, J., Chen, J. K., and Zhang, Y., Theoretical analysis of thermal damage in biological tissues caused by laser irradiation, *Molec. Cell. Biomech.*, vol. 4, pp. 27–39, 2007.